



Deposited via The University of York.

White Rose Research Online URL for this paper:

<https://eprints.whiterose.ac.uk/id/eprint/142815/>

Version: Accepted Version

Article:

Hargreaves, Jessica Kate, Knight, Marina Iuliana, Pitchford, Jonathan William et al. (2019) Wavelet spectral testing: application to nonstationary circadian rhythms. *Annals of Applied Statistics*. pp. 1817-1846. ISSN: 1932-6157

<https://doi.org/10.1214/19-AOAS1246>

Reuse

Items deposited in White Rose Research Online are protected by copyright, with all rights reserved unless indicated otherwise. They may be downloaded and/or printed for private study, or other acts as permitted by national copyright laws. The publisher or other rights holders may allow further reproduction and re-use of the full text version. This is indicated by the licence information on the White Rose Research Online record for the item.

Takedown

If you consider content in White Rose Research Online to be in breach of UK law, please notify us by emailing eprints@whiterose.ac.uk including the URL of the record and the reason for the withdrawal request.

WAVELET SPECTRAL TESTING: APPLICATION TO NONSTATIONARY CIRCADIAN RHYTHMS

BY JESSICA K. HARGREAVES^{*}, MARINA I. KNIGHT^{*}, JON W. PITCHFORD[†],
RACHAEL J. OAKENFULL[‡], SANGEETA CHAWLA[‡], JACK MUNNS[‡] AND SETH J.
DAVIS[‡]

University of York^{*, †, ‡}

Rhythmic data are ubiquitous in the life sciences. Biologists need reliable statistical tests to identify whether a particular experimental treatment has caused a significant change in a rhythmic signal. When these signals display nonstationary behaviour, as is common in many biological systems, the established methodologies may be misleading. Therefore, there is a real need for new methodology that enables the formal comparison of nonstationary processes. As circadian behaviour is best understood in the spectral domain, here we develop novel hypothesis testing procedures in the (wavelet) spectral domain, embedding replicate information when available. The data are modelled as realisations of locally stationary wavelet processes, allowing us to define and rigorously estimate their evolutionary wavelet spectra. Motivated by three complementary applications in circadian biology, our new methodology allows the identification of three specific types of spectral difference. We demonstrate the advantages of our methodology over alternative approaches, by means of a comprehensive simulation study and real data applications, using both published and newly generated circadian datasets. In contrast to the current standard methodologies, our method successfully identifies differences within the motivating circadian datasets, and facilitates wider ranging analyses of rhythmic biological data in general.

1. Introduction. Almost all species exhibit changes in their behaviour between day and night (Bell-Pedersen et al., 2005). These daily rhythms (known as ‘circadian rhythms’) are the result of an internal timekeeping system, in response to daily changes in the physical environment (Vitaterna et al., 2001; Minors and Waterhouse, 2013). The ‘circadian clock’ enhances survival by directing anticipatory changes in physiology synchronised with environmental fluctuations. When an organism is deprived of external time cues, its circadian rhythms typically persist qualitatively but may change in detail; the study of these changes can reveal the biochemical reactions underpinning the circadian clock and, at a

MSC 2010 subject classifications: Primary 62M10, 60G18; secondary 60-08

Keywords and phrases: wavelets, spectral decomposition, hypothesis testing, circadian rhythms

Funding: This work was supported by EPSRC. Circadian work in the SJD group is currently funded by BBSRC awards BB/M000435/1 and BB/N018540/1.

larger scale, can provide valuable insight into the possible consequences of environmental and ecological challenges (McClung, 2006; Bujdoso and Davis, 2013).

1.1. *Motivation.* In many scientific applications, the available data consist of signals with known group memberships and scientists are interested in establishing whether these groups display statistically different behaviour. Our work is motivated by a general problem: biologists need reliable statistical tests to identify whether a particular experimental treatment has caused a significant change in the circadian rhythm. If the changes are limited to period and/or phase then existing Fourier-based theory may be adequate. However, when the changes to the circadian clock are less straightforward, for example involving non-stationarity or changes at multiple scales (Hargreaves et al., 2018), the application of these established methods may be conducive to misleading conclusions. The value of our approach is illustrated by three complementary examples, encompassing the effect of various salt stresses on plants, the identification of mutations inducing rapid rhythms, and the response of nematode clocks to pharmacological treatment, as described in the following sections. The biological experimental details for each dataset appear in Appendix A.

1.1.1. *Lead nitrate dataset (Davis Lab, Biology, University of York).* This dataset (henceforth referred to as the ‘Lead dataset’) is from a broad investigation of whether plant circadian clocks are affected by industrial and agricultural pollutants (Foley et al., 2005; Senesil et al., 1998; Hargreaves et al., 2018; Nicholson et al., 2003). Specifically, this experiment asks whether lead affects the *Arabidopsis thaliana* circadian clock and, if so, when and how? Figure 1 displays the luminescence profiles for both untreated *A. thaliana* plants, as well as for those exposed to lead nitrate.

1.1.2. *Ultradian dataset (Millar Lab, Biology, University of Edinburgh).* In order to understand the clock mechanism, a common approach is to mutate a gene and examine the resulting behaviour in response to a variety of stimuli. Figure 2 depicts the luminescence profiles recording plant response to light for both the control and genetically mutated *A. thaliana* plants (Millar et al., 2015). Researchers are interested in establishing whether a specific genetic mutation induced high-frequency behaviour (known as ‘ultradian rhythms’) in the laboratory model plant *A. thaliana*.

1.1.3. *Nematode dataset (Chawla Lab, Biology, University of York).* The free-living nematode *Caenorhabditis elegans* is an animal widely used in neuroscience and genetics, but its circadian clock is still poorly understood. To increase understanding of the nematode clock, and potentially uncover rhythmicity not

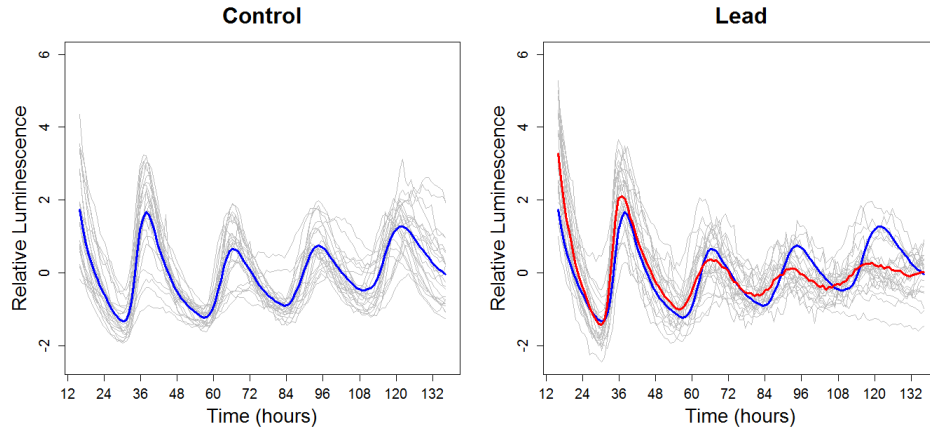


FIG 1. **Lead dataset:** Luminescence profiles over time for untreated *A. thaliana* plants (Control) and those exposed to lead nitrate (Lead). Left: Individuals in the control group (in grey) along with the group average (blue). Right: Individuals in the lead treatment group (in grey) along with the treatment group average (red) and the control group average (blue). Each time series has been re-centred around zero.

detected by conventional approaches, researchers applied a pharmacological treatment to *C. elegans*, based on evidence that it causes aberrant circadian rhythms in other established mammalian and insect circadian models (Kon et al., 2015; Dusik et al., 2014). Figure 3 depicts the luminescence profiles for both untreated and treated *C. elegans*.

On examining Figures 1 and 2, it is visually clear that changes in period and amplitude between the control and test groups occur in both datasets. Figure 3 reveals apparently similar luminescence profiles for both untreated and treated *C. elegans*. Nevertheless, in each experiment, less easily quantified or subtle differences between these groups may also exist.

1.2. *Aims and structure of the paper.* Period estimation is central to the analysis of circadian data, with the current standard achieving this using Fourier analysis (Zielinski et al., 2014; Costa et al., 2011) via software packages, such as BRASS (Biological Rhythm Analysis Software System (Edwards et al., 2010)) or BioDare (Moore et al., 2014). The practitioner estimates the period of the control and treatment groups respectively, and then tests for statistically significant differences (see for example Perea-García et al. (2015), Costa et al. (2011)). Crucially, in all of our motivating examples, such established Fourier-based tests found no significant difference between groups (see Table S1 in Appendix B.1).

One obvious limitation of this analysis is that the employed methodology

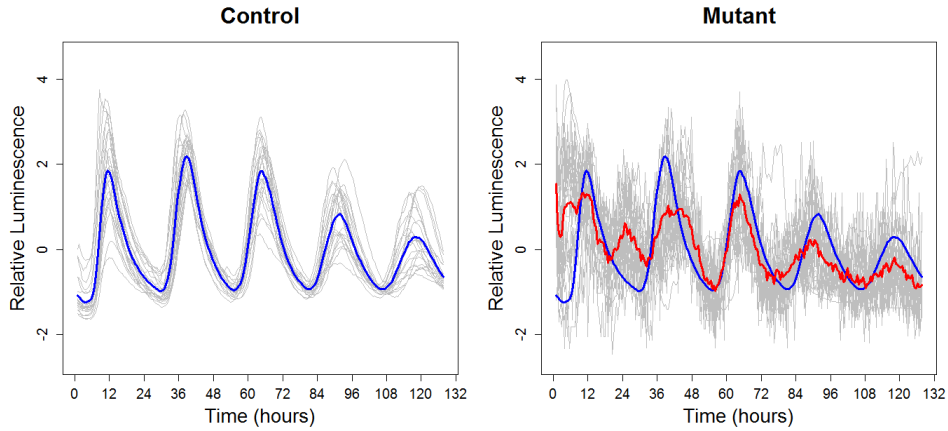


FIG 2. **Ultradian dataset:** Luminescence profiles over time for control and mutant *A. thaliana* plants. Left: Individuals in the control group (in grey) along with the group average (blue). Right: Individuals in the mutant group (in grey) along with the mutant group average (red) and the control group average (blue). Each time series has been re-centred around zero.

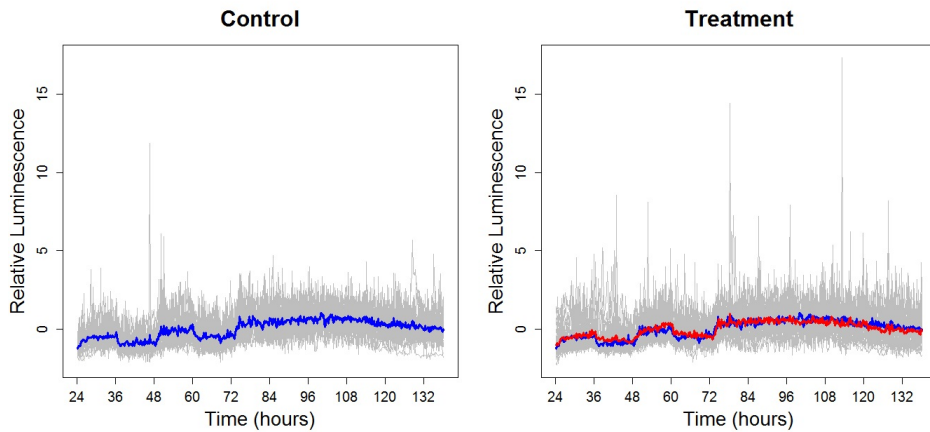


FIG 3. **Nematode dataset:** Luminescence profiles over time for untreated *C. elegans* (Control) and those subjected to a pharmacological treatment (Treatment). Left: Individuals in the control group (in grey) along with the group average (blue). Right: Individuals in the treatment group (in grey) along with the treatment group average (red) and the control group average (blue). Each time series has been re-centred around zero.

does not typically evaluate the crucial underpinning assumption of data stationarity. In the context examined here, assuming stationarity can be inappropriate (Hargreaves et al., 2018; Leise et al., 2013), a feature shared by many biological systems (Zielinski et al., 2014). For our motivating example datasets, we investigated whether the individual time series are (second-order) stationary via hypothesis testing. We employed two tests for stationarity— a Fourier-based test (the Priestley-Subba Rao (PSR) (Priestley and Rao, 1969) test) and a wavelet-based test (Nason, 2013). The results (Table S2 in Appendix B.1) show that, for each of our motivating example datasets, over 80% of the time series provided enough evidence to reject the null hypothesis of stationarity. This result suggests that the application of the current methodology (which assumes data stationarity) would be inappropriate for our motivating datasets and highlights the urgent need for more statistically advanced approaches.

In the specific context of circadian clock data, wavelets have been recognised as ideally suited to identifying local time and scale features (Leise et al., 2013; Harang et al., 2012), with time-scale patterns known as indicative of the organism response to external stimuli (Zielinski et al., 2014). A substantial body of circadian literature advocates the use of wavelet (Zielinski et al., 2014; Leise et al., 2013; Harang et al., 2012) and, in particular, spectral representations (Price et al., 2008) of circadian rhythms. This motivates our choice to formally compare circadian signals in the wavelet spectral domain by using their time-scale signature patterns and thus accounting for their proven nonstationary features. Furthermore, we propose to adopt the locally stationary wavelet (LSW) process model of Nason et al. (2000), which is capable of accounting for data nonstationarity and crucially has previously demonstrated utility for circadian analysis (Hargreaves et al., 2018). Modelling nonstationary data within the LSW framework has also proven successful across a wide variety of fields, from climatology (Fryzlewicz et al., 2003) and ocean engineering (Killick et al., 2013) to medicine (Nason and Stevens, 2015) and finance (Fryzlewicz, 2005) corresponding to a multitude of tasks such as forecasting, change-point detection, spectral estimation and modelling, respectively.

The primary contribution of this work is the development of novel wavelet-based hypothesis tests that allow for circadian behaviour comparison while accounting for data nonstationarity. This article is organised as follows. Section 2 reviews the theoretical wavelet-based framework we adopt for modelling nonstationary data and the relevant literature on hypothesis testing in the spectral domain. Our new hypothesis testing procedures are introduced in Section 3. Section 4 provides a comprehensive performance assessment of our new methods via simulation. Section 5 demonstrates the additional insight our techniques provide for the motivating circadian datasets and Section 6 concludes this work.

2. Overview: nonstationary processes and hypothesis testing in the spectral domain.

2.1. *Modelling nonstationary processes.* Many of the statistically rigorous approaches to modelling nonstationary time series stem from the Cramér-Rao representation of stationary processes that states that all zero-mean discrete time second-order stationary time series $\{X_t\}_{t \in \mathbb{Z}}$ can be represented as

$$(2.1) \quad X_t = \int_{-\pi}^{\pi} A(\omega) \exp(i\omega t) d\xi(\omega),$$

where $A(\omega)$ is the amplitude of the process and $d\xi(\omega)$ is an orthonormal increments process (Priestley, 1982). In the representation of stationary processes above, the amplitude $A(\omega)$ does not depend on time, i.e. the frequency behaviour is the same across time. However, for many real time series, including our circadian datasets, this is unrealistic (Price et al., 2008) and a model where the frequency behaviour can vary with time is needed.

The LSW paradigm provides precisely such a desired setup, and has also proved to yield superior results when compared to competitor methods in useful tasks such as classification (e.g. Krzemieniewska et al. (2014) for aerosol spray data) and clustering (e.g. Hargreaves et al. (2018) for circadian rhythms). Fryzlewicz (2005) brings strong arguments for the utility of (linear) Gaussian LSW models for financial data, typically modelled using (non-linear) models, that allow for time-dependent conditional variance.

In a nutshell, in the LSW framework, the Fourier building blocks in equation (2.1) are replaced by families of discrete nondecimated wavelets and an LSW process $\{X_{t;T}\}_{t=0}^{T-1}$, $T = 2^J \geq 1$ is represented as follows

$$(2.2) \quad X_{t;T} = \sum_{j=1}^J \sum_{k \in \mathbb{Z}} w_{j,k;T} \psi_{j,k}(t) \xi_{j,k},$$

where $\{\xi_{j,k}\}$ is a random orthonormal increment sequence, $\{\psi_{j,k}(t) = \psi_{j,k-t}\}_{j,k}$ is a set of discrete non-decimated wavelets and $\{w_{j,k;T}\}$ is a set of amplitudes, each of which at a scale j and time k . Within each scale j , the amplitudes $\{w_{j,k;T}\}_k$ are regulated by a Lipschitz continuous function $W_j(k/T)$, which further fulfils some technical assumptions in order to allow estimation. Appendix C provides the background details.

2.1.1. *Practical considerations.* In this paper, we assume the innovations $\{\xi_{j,k}\}$ to be normally distributed, resulting in modelling the data $\{X_{t;T}\}$ as a Gaussian LSW process. The normality assumption is typically employed for the (Fourier) circadian testing methodology (Perea-García et al., 2015). This assumption is

also commonly made in time series analysis in general and in LSW modelling in particular (e.g. [Oh et al. \(2003\)](#), [Van Bellegem and von Sachs \(2008\)](#) and [Nason and Stevens \(2015\)](#)), with [Nason \(2013\)](#) arguing for its non-limiting character in this context. In [Appendix B.2](#) we show this assumption is tenable for our circadian datasets.

The properties of the random increment sequence $\{\xi_{j,k}\}$ ensure that $\{X_{t,T}\}$ is a zero-mean process. In practice, for a process with non-zero mean, it is customary to re-centre it around zero ([Nason, 2010](#)) and this is our approach here, as the quantity of our primary interest is the process spectral signature.

As is typical for wavelet representations, the data is often required to be of dyadic length, $T = 2^J$. In many practical applications, this is not realistic and there are a number of approaches to address this situation (see e.g. [Ogden \(1997\)](#)). Our approach is to analyse a (dyadic length) segment of the data, with the truncation decided upon careful consultation with the experimental scientists in order to ensure the time-frame of interest is represented.

2.1.2. The evolutionary wavelet spectrum. Under the LSW framework, a quantity analogous to the spectrum of a stationary process is the evolutionary wavelet spectrum (EWS) $S_j(z) := |W_j(z)|^2$, at each scale $j \in \overline{1, J}$ and rescaled time $z = k/T \in (0, 1)$. The EWS quantifies the power distribution in the process over time and scale. We define the raw wavelet periodogram as $I_{j,k;T} = |d_{j,k;T}|^2$, where $d_{j,k;T} = \sum_{t=0}^T X_{t,T} \psi_{j,k}(t)$ are the empirical nondecimated wavelet coefficients. In the remainder of this paper we drop the explicit dependence on T for the wavelet coefficients and the periodogram.

The raw wavelet periodogram is an asymptotically unbiased estimator of the quantity

$$(2.3) \quad \beta_j(z) = \sum_{i=1}^J A_{i,j} S_i(z) = (AS)_j(z),$$

where $A = (A_{i,j})_{i,j=1}^J = (\sum_{\tau} \Psi_i(\tau) \Psi_j(\tau))_{i,j=1}^J$ is the autocorrelation wavelet inner product matrix, with $\Psi_j(\tau) = \sum_k \psi_{j,k}(0) \psi_{j,k}(\tau)$ the autocorrelation wavelet ([Nason et al., 2000](#)). The quantity $\beta_j(z)$ was introduced by [Fryzlewicz and Nason \(2006\)](#) and is often easier to work with theoretically than the spectrum ([Nason, 2013](#)). An asymptotically unbiased estimator of the EWS is the empirical wavelet spectrum:

$$(2.4) \quad \mathbf{L}(z) := A^{-1} \mathbf{I}(z),$$

for all $z \in (0, 1)$, where $\mathbf{I}(z) := (I_{j,[zT]})_{j=1}^J$ is the raw wavelet periodogram vector.

The empirical wavelet spectrum is a collection of random variables that are not independent, nor is their (joint or marginal) distribution easy to determine.

As each coefficient of the empirical wavelet spectrum is a sum of a (typically logarithmic) number of terms (see equation (2.4)), a mechanism similar to the central limit theorem brings it closer to normality than the raw wavelet periodogram (Fryzlewicz and Ombao, 2009), which is distributed as a scaled χ_1^2 . As the individual raw periodogram ordinates within each scale are correlated, Fryzlewicz and Nason (2006) model the raw wavelet periodogram as approximately

$$I_{j,k} \sim \beta_j(z) Z_{j,k}^2,$$

where $z = k/T$ and $Z_{j,k}^2 \sim \chi_1^2$, for $j \in \mathbb{N}$, $k = 0, \dots, 2^j - 1 = T - 1$.

A way to ‘correct’ these undesirable features is to employ a transform that brings the raw periodogram ordinates closer to Gaussianity and decorrelates within each scale. We adopt the Haar-Fisz transform (denoted \mathcal{F}), introduced (for spectral estimation) by Fryzlewicz and Nason (2006) and apply it separately to each scale $j = 1, \dots, J$ of the raw wavelet periodogram, denoted $\mathcal{H}_{j,k;T} := \mathcal{F} I_{j,k;T}$. Proposition 4 in Fryzlewicz and Nason (2006) then suggests a potential model

$$\mathcal{H}_{j,k} \sim N(\mathcal{B}_j(z), \sigma_j^2),$$

where $\mathcal{B}_j(z) = \mathcal{F} \beta_j(z)$ with $z = k/T$ and $\mathcal{F} Z_{j,k}^2$ are approximately uncorrelated $N(0, \sigma_j^2)$, again dropping the explicit dependence on T . This model, viewed as a nonparametric additive regression model, was also employed by Nason and Stevens (2015) in the context of Bayesian spectral estimation, where its viability was demonstrated.

2.2. Spectral domain hypothesis testing. Assuming that the available data consists of multiple nonstationary time series with known group memberships, to the authors’ knowledge no hypothesis tests exist to determine whether two groups are significantly different in terms of their associated (evolutionary) wavelet spectra. Wavelet spectral comparison is closest framed as a (consistent) classification method by Fryzlewicz and Ombao (2009), further improved by Krzemińska et al. (2014). Spectral comparison, framed as testing for spectral constancy, also appears in connection with testing for time series stationarity and white noise testing. In the Fourier domain, Priestley and Rao (1969) determined (as a hypothesis test) whether the spectrum is time-varying and, hence, whether the process is nonstationary. Von Sachs and Neumann (2000) introduced the principle of assessing the constancy of the time-varying Fourier spectrum by examining its Haar wavelet coefficients across time. In the wavelet domain, Nason (2013) developed a test for second-order stationarity which examines the constancy of a wavelet spectrum by also examining its Haar wavelet coefficients. A similar approach is adopted by Nason and Savchev (2014) in the development of white noise tests.

The problem of testing that involves curves is often posed in time series literature as a functional regression problem defined using a functional response and categorical predictors (functional ANOVA; see the monograph of [Ramsay and Silverman \(2005\)](#) for its introduction and the review of [Morris \(2015\)](#) for developments in the field). Functional regression problems are often treated by projection in the Fourier or wavelet domain, where the spectral time series representations become subject to modelling. [Shumway \(1988\)](#) compares groups of curves (with stationary stochastic errors) by testing whether the mean curves have the same Fourier spectrum at each given frequency. [Fan and Lin \(1998\)](#) developed this method by applying the adaptive Neyman test to the (Fourier or wavelet) transformed difference vector (the difference between the two group-average time series). [Vidakovic \(2001\)](#) introduces a wavelet-based functional data analysis, with [McKay et al. \(2012\)](#) developing this as an approach for comparing neurophysiological signals that are functions of time. This approach was also subsequently adopted by [Atkinson et al. \(2017\)](#) to develop model validation using a test statistic based on thresholded wavelet coefficients. [Tavakoli and Panaretos \(2016\)](#) compare pairs of stationary functional time series by developing t -tests for the equality of their (Fourier) spectral density operators. However, these approaches fail to account for potential nonstationarity in the data. This is mitigated by [Guo et al. \(2003\)](#), who propose a smoothing-spline ANOVA on the logarithm of the Fourier spectrum of a locally stationary process that is specifically designed to discriminate between models that contain a linear trend, modulation, time and frequency interaction terms, thus yielding global model comparisons, rather than time- and frequency-specific ones. The closest methodology for spectral comparison while allowing for a localised representation comes from [Martinez et al. \(2013\)](#) who identify regional differences in (the Fourier spectrograms of) bat mating chirps. The statistical modelling of windowed Fourier spectrograms as an image was first proposed by [Holan et al. \(2010\)](#) in a study that aimed to classify animal communication signals. [Martinez et al. \(2013\)](#) apply the higher-dimension functional mixed model of [Morris et al. \(2011\)](#) and use a Bayesian approach to fit a model that incorporates localised chirp Fourier spectrograms as the functional response and categorical regressors that identify bat location (fixed-effects) and independent bat (random)-effects. The observed data is modelled in a (projected) wavelet-domain with several distributional assumptions in place, e.g. data Gaussianity, spike Gaussian-slab prior distributions for the wavelet coefficients. However, while their windowed Fourier spectrogram does offer a time-frequency representation of the data, thus potentially capturing nonstationarity, it is sensitive to the choice of kernel and crucially of window-width ([Martinez et al., 2013](#)). In the context of clustering circadian plant rhythms, [Hargreaves et al. \(2018\)](#) demonstrated the superiority of a principled

model-based spectral estimator that, in the spirit of [Holan et al. \(2010\)](#), was also used as an image in subsequent modelling. Additionally, we note that our study aims to identify not only (i) time-scale (frequency) group differences (conceptually a task close to [Martinez et al. \(2013\)](#)), but also (ii) to detect global scale-level differences (while still allowing for a development that incorporates potential nonstationarity) and (iii) to identify similar patterns within each scale, rather than exact differences (the reader will find precise details in the next section).

3. Proposed spectral domain hypothesis tests. Aligned to our motivating examples, the key goals of our work are to develop novel hypothesis tests, each capable of detecting one of three specific types of spectral differences between two groups and to identify the scales and times (e.g. Lead and Nematode datasets—Sections 1.1.1 and 1.1.3) or scales only (e.g. Ultradian dataset—Section 1.1.2) at which these difference arise, as appropriate.

Formally, recall that we model the observed nonstationary circadian rhythms as (Gaussian) LSW processes, using the framework of [Nason et al. \(2000\)](#) (see Section 2.1 and Appendix C for details). Within our motivating datasets, the data naturally shared the same starting point (see Appendix A). As our methodological development is motivated by experimental data, we assume all signals are of a common length T . Thus denote each individual profile by $\{X_{t,T}^{(i),r_i}\}_{t=0}^{T-1}$ with $i = 1, 2$ corresponding to one of two groups (e.g. control/ treatment) and potential replicates $r_i = 1, \dots, N_i$ (i.e. N_i circadian traces in the i th group). Note that when $N_i = 1$ we drop the r_i index for simplicity. Assume the signals in group i are underpinned by a common wavelet spectrum and denote this by $S_j^{(i)}(t/T)$ for each group $i = 1, 2$ at scales $j \in \overline{1, J}$ ($J = \log_2 T$) and rescaled times $z = t/T \in (0, 1)$.

3.1. *Lead dataset: Hypothesis testing for spectral equality ('WST' and 'FT').* Put simply, our soil pollutant example focussed on detecting whether the two plant groups, 'Control' and 'Lead', display significant differences in the evolution of their spectral structures, and if so, the particular scales and times at which such differences occur. Mathematically we formalise our hypotheses as

$$(3.1) \quad H_0 : S_j^{(1)}(z) = S_j^{(2)}(z), \quad \forall j, z$$

versus the alternative $H_A : S_{j^*}^{(1)}(z^*) \neq S_{j^*}^{(2)}(z^*)$ for some scale j^* and rescaled time z^* . In the time domain, we visually note that differences in the circadian rhythms of the two groups appear towards the end of the experiment (see Figure 1).

3.1.1. *A naive wavelet spectrum test ('WST').* Since in reality we do not know the group spectrum $S_j^{(i)}(z)$, we replace it with a well-behaved estimator, denoted

$\hat{S}_j^{(i)}(z)$. Assuming independent replicates are available for each group, we use the group ($i = 1, 2$) averaged spectral estimators

$$(3.2) \quad \hat{S}_j^{(i)}(k/T) = \frac{1}{N_i} \sum_{r_i=1}^{N_i} L_j^{(i),r_i}(k/T),$$

where $L_j^{(i),r_i}(k/T)$ is the empirical wavelet spectrum of the r_i th series in group i at scale j and time k . Assuming independence across the replicates and a Gaussian distribution for the spectral estimates, because the LSW theory constructs asymptotically unbiased spectral estimators, it follows that under the null hypothesis $\hat{S}_j^{(1)}(k/T) - \hat{S}_j^{(2)}(k/T)$ has an asymptotically normal distribution with mean zero. Hence, should our spectral estimators satisfy the classical assumptions for a t -test (which in our context amount to independence of the spectral estimates across replicates and a Gaussian distribution), we propose a naive *wavelet spectrum test* (WST), centred on a test statistic of the form

$$(3.3) \quad T_{j,k} = \frac{\hat{S}_j^{(1)}(k/T) - \hat{S}_j^{(2)}(k/T)}{\left((\hat{\sigma}_{j,k}^{(1)})^2 / N_1 + (\hat{\sigma}_{j,k}^{(2)})^2 / N_2 \right)^{1/2}} \sim t_{df} \text{ under the null hypothesis,}$$

where $(\hat{\sigma}_{j,k}^{(i)})^2$ is an estimate of the variance of $\hat{S}_j^{(i)}(k/T)$ for $i = 1, 2$ across the N_i observations in group i , obtained using the standard sum-of-squares sample variance formula (as in Krzemieniewska et al. (2014)). Under the null hypothesis of spectral equality, $T_{j,k}$ (asymptotically) follows a t -distribution with the number of degrees of freedom (df) directly related to the variance estimation procedure we employ. Each test statistic is then compared with a critical value derived from the t -distribution in the usual way.

When the variance of $\hat{S}_j^{(i)}(k/T)$ is unknown but common to both $i = 1, 2$ groups (denoted $(\sigma_{j,k})^2 := (\sigma_{j,k}^{(1)})^2 = (\sigma_{j,k}^{(2)})^2$), it can be estimated using the pooled estimator:

$$(3.4) \quad \hat{\sigma}_{j,k}^2 = \frac{(N_1 - 1)(\hat{\sigma}_{j,k}^{(1)})^2 + (N_2 - 1)(\hat{\sigma}_{j,k}^{(2)})^2}{N_1 + N_2 - 2},$$

replacing $(\hat{\sigma}_{j,k}^{(1)})^2$ and $(\hat{\sigma}_{j,k}^{(2)})^2$ in equation (3.3). The number of degrees of freedom in the t -distribution of the test statistic is then $df = N_1 + N_2 - 2$.

If there is no reason to believe the group variances are equal, then use a t -distribution with degrees of freedom

$$df = \frac{\left((\hat{\sigma}_{j,k}^{(1)})^2 / N_1 + (\hat{\sigma}_{j,k}^{(2)})^2 / N_2 \right)^2}{\frac{(\hat{\sigma}_{j,k}^{(1)})^2 / N_1}{N_1 - 1} + \frac{(\hat{\sigma}_{j,k}^{(2)})^2 / N_2}{N_2 - 1}}.$$

However, the test statistic does not exactly follow the t -distribution, since two standard deviations are estimated in the statistic. Conservative critical values may also be obtained by using the t -distribution with N degrees of freedom, where N represents the smaller of N_1 and N_2 (Moore, 2007).

In practice, the spectral estimators in equation (3.2) may breach the Gaussianity testing assumption, especially when only a low number of replicates are available. The assumption of approximate normality for individual replicate spectral estimates, cautiously used in Fryzlewicz and Ombao (2009), will be strengthened by the presence of a higher collection of group replicates (N_1, N_2) (see Section 4 for a discussion of WST's features and caveats).

3.1.2. *Raw periodogram F-Test ('FT')*. We now construct a testing procedure that is not reliant on the Gaussianity assumption whose validity we challenged above. Formally, for each scale $j \in \mathbb{N}$ and rescaled time $z \in (0, 1)$, the spectral equality $S_j^{(1)}(z) = S_j^{(2)}(z)$ is equivalent to $\beta_j^{(1)}(z) = \beta_j^{(2)}(z)$ as the autocorrelation wavelet inner product matrix A that links the two (see equation (2.3)) is invertible. We therefore replace our initial collection of multiple hypothesis tests with equivalent re-framed versions

$$H_0 : \beta_j^{(1)}(z) = \beta_j^{(2)}(z), \forall j, z$$

against the alternative (H_A) that there exist a scale j^* and rescaled time z^* such that $\beta_{j^*}^{(1)}(z^*) \neq \beta_{j^*}^{(2)}(z^*)$. In order to construct our test statistic, we test for spectral equality by examining the $\beta_j(z)$ quantities instead.

In reality we do not know $\beta_j^{(i)}(z)$ for $i = 1, 2$ so we replace it by an asymptotically unbiased estimator. As data are available consisting of multiple time series with known group memberships, we replace $\beta_j^{(i)}(z)$ with an estimate across the group replicates. Specifically, if we have N_i independent time series replicates from group i , we define

$$(3.5) \quad N_i \bar{I}_{j,k}^{(i)} := \sum_{r=1}^{N_i} I_{j,k}^{(i),r_i} \sim \beta_j^{(i)}(k/T) \chi_{N_i}^2.$$

The distribution above follows as the raw wavelet periodogram coefficient of each r_i th periodogram replicate $I_{j,k}^{(i),r_i}$ is approximately (scaled) χ_1^2 distributed (e.g. Nason and Stevens (2015)) and independent of all other raw wavelet periodogram coefficients across all other replicates from the same group (also see Fryzlewicz and Ombao (2009) and the discussion in Section 2.1). Under the further assumption of group independence, $\bar{I}_{j,k}^{(1)}$ and $\bar{I}_{j,k}^{(2)}$ are independent and distributed as detailed in equation (3.5). Hence we propose the test statistic

$$(3.6) \quad F_{j,k} = \frac{\bar{I}_{j,k}^{(1)}}{\bar{I}_{j,k}^{(2)}} \sim F_{N_1, N_2} \text{ under the null hypothesis.}$$

Each test statistic is then compared with a critical value derived from the F_{N_1, N_2} -distribution in the usual way.

Discussion. An advantage of the FT, particularly as opposed to the WST, is that its underlying distributional assumption is theoretically, as well as practically, more reliable. We would therefore expect the FT to outperform the WST in many applications, and this is indeed validated across a variety of simulation settings (see Section 4).

As we wish to test many hypotheses of the type $H_0 : \beta_j^{(1)}(k/T) = \beta_j^{(2)}(k/T)$ for several values of j and k , we are in the field of multiple-hypothesis testing. For all tests we develop, we use Bonferroni correction and, for a less conservative approach, the false discovery rate (FDR) procedure introduced by [Benjamini and Hochberg \(1995\)](#). Our simulations in Section 4 show that both these methods work well. However, of course the tests themselves are related to one another, but just as in [Nason \(2013\)](#) we do not pursue this topic further in this work.

The WST and FT developed above both report the time-scale locations of the significant differences between the two group spectra. These can be visualised as a ‘barcode’ plot, where a significant difference is represented by a black line at the time-scale location of the rejection of the null hypothesis (see for example Figure 4, right). Alternatively, for all our proposed tests, practitioners can also be informed by the number of rejections (as a dissimilarity measure), with larger values indicating a greater departure from the null hypothesis (as discussed in [Das and Nason \(2016\)](#) and in Section 4.2).

3.2. *Ultradian dataset: Hypothesis testing for spectral equality across scales (HFT).* For certain biological applications, such as the Ultradian motivating example, it is more important to identify spectral differences between groups at scale-level and the time locations of spectral differences are of less interest. For such situations, we replace the spectral comparison $H_0 : S_j^{(1)}(z) = S_j^{(2)}(z)$ of the previous section, in general equivalent to $H_0 : \beta_j^{(1)}(z) = \beta_j^{(2)}(z)$, by the comparison of the respective Haar-Fisz transforms, i.e. test for

$$H_0 : \mathcal{F} \beta_j^{(1)}(z) = \mathcal{F} \beta_j^{(2)}(z), \forall j, z.$$

Equivalently, in the notation established in Section 2.1 we test

$$(3.7) \quad H_0 : \mathcal{B}_j^{(1)}(z) = \mathcal{B}_j^{(2)}(z), \forall j, z$$

versus the alternative (H_A) that there exist some scale j^* and rescaled time z^* for which the equality does not hold. We shall refer to this test as the *Haar-Fisz test* (HFT). Intuitively, although the HFT identifies both scales and times at which the null hypothesis of spectral equality in the Haar-Fisz domain does not hold,

as the Haar-Fisz transform essentially ‘averages’ within each scale of the raw wavelet periodogram, potential differences ‘spread’ throughout the scale. This property makes it ideal for identifying scale-level differences between group wavelet spectra (see for example Figure 5, right).

As we do not know $\mathcal{B}_j^{(i)}(z)$, we replace it by its approximately unbiased estimator $\mathcal{H}_{j,k}^{(i)}$ at scale j and time k (with $z = k/T$) for group $i = 1, 2$. In applications which do not provide access to replicate data, we could adopt equation (3.3) with $\hat{S}_j^{(i)}(k/T)$ replaced by $\mathcal{H}_{j,k}^{(i)}$ and estimate the variance across each scale as the Haar-Fisz transform stabilises variance (Nason and Stevens, 2015) (see Appendix D). When replicates are available, we use equation (3.2) with $\mathcal{H}_{j,k}^{(i)}$ to obtain group averaged estimators of $\mathcal{B}_j^{(i)}(z)$, denoted $\hat{\mathcal{H}}_{j,k}^{(i)}$, and propose a test statistic as in equation (3.3) with $\hat{S}_j^{(i)}(k/T)$ replaced by $\hat{\mathcal{H}}_{j,k}^{(i)}$. The variance estimation techniques and subsequent test statistic distribution follow as detailed in Section 3.1 and the results of the HFT can also be visualised as a ‘barcode’ plot.

The rationale of this approach is also to bring the data (in this context, the Haar-Fisz transform of the raw wavelet periodogram) closer to Gaussianity and to break the dependencies across time. Consequently, the assumptions behind the t -test are closely adhered to and the dependencies between the multiple tests we perform are weak. In practice, due to its scale averaging construction, the HFT unsurprisingly results in many more time-localised rejections than the actual number of differing coefficients in the original spectra, and does sometimes have difficulty discriminating between spectra which differ by a small number of coefficients; however, the HFT does correctly identify scale-level spectral differences (see Section 4 for further investigations).

3.3. *Nematode dataset: Hypothesis testing for ‘same shape’ spectra (‘HT’)*. In applications such as the Nematode example, the focus may be on identifying whether groups evolve according to spectra that have the same shape at each scale, thus indicating that the same patterns are identified in the data, albeit with potentially different magnitudes.

Mathematically, for a scale-dependent (non-zero) constant denoted by C_j , we formalise our hypotheses as

$$(3.8) \quad H_0 : S_j^{(1)}(z) = S_j^{(2)}(z) + C_j, \quad \forall j, z$$

versus the alternative $H_A : S_{j^*}^{(1)}(z^*) \neq S_{j^*}^{(2)}(z^*) + C_{j^*}$ for some scale j^* and time z^* .

Denoting by \underline{C} the $J \times 1$ vector that holds C_j as its j th component and recalling equation (2.3), we can equivalently re-frame the problem into testing whether

$$H_0 : \beta_j^{(1)}(z) = \beta_j^{(2)}(z) + c_j, \text{ or equivalently } H_0 : \beta_j^{(D)}(z) = c_j, \quad \forall j, z$$

where c_j is the j th entry of the vector $\underline{c} = AC$ and $\beta_j^{(D)}(z) := \beta_j^{(1)}(z) - \beta_j^{(2)}(z)$.

In the spirit of the tests developed in [Fan and Lin \(1998\)](#), and as undertaken by [Von Sachs and Neumann \(2000\)](#) and [Nason \(2013\)](#), at each scale j we assess the constancy through time of $\beta_j^{(D)}(z)$ by examining its associated Haar wavelet coefficients. Although, in principle, any wavelet system could be adopted, [Von Sachs and Neumann \(2000\)](#) note that the Haar wavelet coefficients are ideal for testing the constancy of a function. Hence we employ these wavelets and refer to the test developed in this section as the *Haar Test* (HT).

The underlying principle behind these tests is that the wavelet transform of a constant function is zero, hence under H_0 above, the wavelet coefficients of $\beta_j^{(D)}(z)$ are

$$v_{\ell,p}^j = \int_0^1 \beta_j^{(D)}(z) \psi_{\ell,p}^H(z) dz = c_j \int_0^1 \psi_{\ell,p}^H(z) dz = 0,$$

where $\{\psi_{\ell,p}^H(z)\}_{\ell,p}$ denote the usual Haar wavelets at scale ℓ and location p .

This suggests performing multiple hypothesis testing on the collection of hypotheses

$$H_0: v_{\ell,p}^j = 0, \forall j, \ell \text{ and } p$$

against the alternative (H_A) that there exist j^* , ℓ^* and p^* such that $v_{\ell^*,p^*}^{j^*} \neq 0$.

As the spectral and related quantities are unknown, and since the wavelet transform is linear, we estimate each $v_{\ell,p}^j$ by $\hat{v}_{\ell,p}^j = \hat{v}_{\ell,p}^{j,(1)} - \hat{v}_{\ell,p}^{j,(2)}$, with the Haar wavelet coefficients corresponding to each group $i = 1, 2$ estimated in the spirit of [Nason \(2013\)](#) as

$$(3.9) \quad \hat{v}_{\ell,p}^{j,(i)} = 2^{-\ell/2} \left(\sum_{r=0}^{2^{\ell-1}-1} I_{j,2^\ell p-r}^{(i)} - \sum_{q=2^{\ell-1}}^{2^\ell-1} I_{j,2^\ell p-q}^{(i)} \right),$$

at each (original) scale j and Haar scale ℓ and locations p, q .

With the availability of independent replicates within each group, we estimate the group i Haar wavelet coefficients as

$$(3.10) \quad \hat{v}_{\ell,p}^{j,(i)} = \frac{1}{N_i} \sum_{r_i=1}^{N_i} \hat{v}_{\ell,p}^{j,(i),r_i},$$

where each $\hat{v}_{\ell,p}^{j,(i),r_i}$ is obtained as in equation (3.9) for the r_i -th replicate.

Under a specific set of assumptions, [Nason \(2013\)](#) shows the asymptotic normality of the Haar wavelet coefficient estimator of the wavelet periodogram at scale j . Thus, in our setting, each $\hat{v}_{\ell,p}^{j,(i),r_i}$ for $i = 1, 2$ is asymptotically normal with mean $v_{\ell,p}^{j,(i),r_i}$ and variance $(\sigma_{\ell,p}^{j,(i)})^2$. Using the replicate independence, we

have that $\hat{v}_{\ell,p}^{j,(i)}$ is asymptotically normally distributed with mean $v_{\ell,p}^{j,(i)}$ and variance $(\sigma_{\ell,p}^{j,(i)})^2/N_i$ and note that its distributional closeness to the normal increases via a central limit theorem argument with the increasing number of replicates.

The group independence assumption then leads to an asymptotically joint normal distribution for $(\hat{v}_{\ell,p}^{j,(1)}, \hat{v}_{\ell,p}^{j,(2)})$. Following the continuous mapping theorem, we obtain that $\hat{v}_{\ell,p}^j = \hat{v}_{\ell,p}^{j,(1)} - \hat{v}_{\ell,p}^{j,(2)}$ has an asymptotic normal distribution with mean $v_{\ell,p}^{j,(1)} - v_{\ell,p}^{j,(2)}$ and variance $(\sigma_{\ell,p}^{j,(1)})^2/N_1 + (\sigma_{\ell,p}^{j,(2)})^2/N_2$.

In the presence of replicates, we propose a test statistic of the form discussed in equation (3.3)

$$(3.11) \quad T_{\ell,p}^j = \frac{\hat{v}_{\ell,p}^j}{\left((\hat{\sigma}_{\ell,p}^{j,(1)})^2/N_1 + (\hat{\sigma}_{\ell,p}^{j,(2)})^2/N_2\right)^{1/2}} \sim t_{df} \text{ under the null hypothesis,}$$

where $(\hat{\sigma}_{\ell,p}^{j,(i)})^2$ is an estimate of the variance of $\hat{v}_{\ell,p}^{j,(i)}$ for $i = 1, 2$ across the N_i observations in group i , obtained using the standard sum-of-squares sample variance formula and df denotes the degrees of freedom associated with the variance estimation procedure (see Section 3.1.1). Each test statistic is then compared with a critical value derived from the t -distribution in the usual way.

In order to control the asymptotic bias derivation, one of the assumptions under which the distributional theory is derived consists of limiting the scales of the Haar wavelet coefficients $v_{\ell,p}^j$ to be sufficiently coarse, $\ell = 0, \dots, (J - \lceil J/2 \rceil - 2)$. Furthermore, as in [Nason \(2013\)](#), we only consider the wavelet coefficients of the periodogram at levels $j \geq 3$ in order to avoid the effects of a region similar to the ‘cone of influence’ described by [Torrence and Compo \(1998\)](#).

To aid the visualisation of the WST, FT and HFT results, we use a ‘barcode’ plot that indicates the time- and scale- locations where significant differences are present. The HT can also indicate where the significant differences are located in the series and can plot the results in a manner similar to the wavelet test of stationarity (see [Nason \(2013\)](#)). However, due to its construction, these locations are more difficult to interpret than for the WST, FT and HFT (see [Figure 6](#)).

4. Simulation studies. The goals of the simulation studies were: (1) to evaluate the empirical power and size of our new tests; (2) to consider the effect of sample size on the accuracy of the tests; (3) to investigate two approaches to multiple-hypothesis testing: Bonferroni correction (denoted ‘Bon.’) and the false discovery rate procedure (‘FDR’); (4) to investigate the performance of our proposed tests when certain modelling assumptions are broken and (5) to evaluate the empirical power and size of our new tests in comparison with the adap-

tive Neyman Test (ANT) of [Fan and Lin \(1998\)](#) (see Section 2.2). This benchmark method performs well in practice when the assumption that the data can be modelled as a functional time series is valid.

In this section we briefly outline the basic structure of each simulated experiment (a comprehensive description of the simulation studies can be found in Appendix D). In each case, we assumed that the signal was a realisation from one of $i = 1, 2$ possible groups. For each group, we generated a set of $N_1 = N_2 = 1, 10, 25, 50$ signal realisations of common length $T = 256$, the equivalent of a free-running period of 4 days. For each realisation, we obtained the raw and corrected wavelet periodograms using (unless otherwise stated) the Haar wavelet (from the `locits` software package for R- available from the CRAN package repository), although, any wavelet system can, in principle be used (see Section 4.3). The Haar-transformed and Haar-Fisz transformed raw wavelet periodogram were subsequently obtained and the spectral testing procedures carried out as described in Section 3. The results are compared with the known group memberships, and the procedure is then repeated 1000 times to obtain empirical size and power estimates as outlined in the following sections.

4.1. *Power comparisons.* To explore statistical power we simulate a set of $N_1 = N_2 = 1, 10, 25, 50$ signal realisations from each group where the individual group spectra are defined such that there exists a scale j^* and time t^* such that $S_{j^*}^{(1)}(t^*/T) \neq S_{j^*}^{(2)}(t^*/T)$. The empirical power estimates are obtained by counting the number of times our tests reject the null hypothesis of spectral equality. The models we will use are denoted **P1–P12** respectively and are briefly described below (details can be found in Appendix D).

1. **P1: Fixed Spectra.** We follow [Krzemieniewska et al. \(2014\)](#) and design the spectra of the two groups to differ at the finest level (resolution level 7) by 100 coefficients.
2. **P2: Fixed Spectra-Fine Difference.** We modify the model **P1** by fixing “Group 1” but defining the spectrum of “Group 2” such that the spectra of the two groups now differ by only 6 coefficients.
3. **P3: Fixed Spectra-Plus Constant.** Modify the model **P1** by fixing “Group 1” but defining the spectrum of “Group 2” such that the spectra of the two groups differ by a constant in the finest resolution level.
4. **P4/P5: Gradual Period Change.** This study replicates a typical circadian experiment with changes that cannot be captured by standard analyses assuming stationarity and only reporting an average period value. We thus define 3 possible groups, where each group represents a signal that gradually changes period from 24 to: 25 (Group 1), 26 (Group 2) and 27 (Group 3) over (approximately) two days, before continuing with the relevant pe-

Model	WST (Bon.)	WST (FDR)	FT (Bon.)	FT (FDR)	HFT (Bon.)	HFT (FDR)	HT (Bon.)	HT (FDR)
P1	100.0	100.0	100.0	100.0	100.0	100.0	100.0	100.0
P2	39.3	48.0	100.0	100.0	29.1	31.8	86.2	86.4
P3	100.0	100.0	100.0	100.0	100.0	100.0	4.3	4.4
P4	1.0	2.7	45.5	54.5	33.2	36.5	100.0	100.0
P5	5.9	14.6	97.0	99.9	100.0	100.0	100.0	100.0
P6	100.0	100.0	87.5	92.6	44.8	89.1	66.5	67.7
P7	100.0	100.0	54.3	64.5	97.4	99.9	100.0	100.0

TABLE 1

Simulated power estimates (%) for models P1-P7 with nominal size of 5% with $N_1 = N_2 = 25$ realisations from each group. Highest empirical power estimates are highlighted in bold.

riod for a further two days (also see [Hargreaves et al. \(2018\)](#)). To determine which changes can be discriminated by the methods, we perform two studies within this setting: simulations from Groups 1 and 2 (**P4**) and simulations from Groups 1 and 3 (**P5**).

- P6/P7: AR Processes with time-varying coefficients.** We simulate from an important class of nonstationary processes—AR(2) processes with: abruptly (**P6**) and slowly (**P7**) changing parameters (as in [Fryzlewicz and Ombao \(2009\)](#)).
- P8–P12: Functional Time Series (Constant Period).** This study follows [Zielinski et al. \(2014\)](#) and generates each time series using an underlying cosine curve with additive noise, which also coincides with the theoretical assumptions of the ANT. We define time series as realisations from one of 6 possible groups, each with a different (constant) period, relevant to our circadian setting. To determine which period changes can be discriminated by the methods, we perform five studies within this setting: simulations from a group with a period of 24 hours versus a group with a period of 21, 22, 23, 23.5 and 23.75 hours (models **P8–P12** respectively).

4.1.1. *Discussion of findings.* The empirical power values for $N_1 = N_2 = 25$ (this is the typical number of available replicates in circadian studies, see [Appendix A](#)) for models **P1–P7** are reported in [Table 1](#). We found that all tests perform well when the spectra differ by a large number of coefficients (model **P1**). The FT (and, to a lesser extent, the HT) are able to discriminate between spectra that differ by a small number of coefficients (model **P2**) whereas the HFT has lower empirical power. By construction, the HT cannot differentiate between spectra that differ by a constant at a particular resolution level (model **P3**), but we found that the HT performs well in our synthetic circadian example of gradual small period change across many time-scale locations (models **P4** and **P5**).

Due to the higher distributional reliability of the FT, it unsurprisingly outperforms the WST when the times series are generated from a defined spectrum (models **P1–P5**). However, distributional properties of the time-varying AR process ensure that the WST performs best when data are generated using models **P6** and **P7**, with the HT and HFT also performing well for model **P7**.

Effect of Sample Size. The number of replicates in each group (N_1, N_2) are also an important factor in achieved power. The results for the HFT with $N_1 = N_2 = 1$ are shown in Table S6 (Appendix D.2), since we recall that the HFT is the only proposed test which can be applied when replicate data is not available—see Section 3.2. The results for all tests with $N_1 = N_2 = 10$ and 50 replicates are shown in Table S7 (Appendix D.2). Increasing the number of replicates should, and indeed does, increase the empirical power of all tests (with the exception of the HT for model **P3**). For example, note the increase in empirical power (particularly for models **P2** and **P4**) as the number of replicates increases from 10 to 25.

Approach to Multiple-hypothesis Testing. These studies show that the Bonferroni correction provides a more conservative approach. The false discovery rate gives an empirical power greater than (or equal to) that of the Bonferroni correction (see e.g. model **P6** in Table 1).

Performance Comparison. We also report that the empirical power of the ANT for model **P5** (gradual period change, 25 replicates) was 10.7%, which is below the results in Table 1 for our proposed tests. This is to be expected as the underlying assumptions of the ANT are no longer met. (Similar results are obtained for models **P1–P7**, hence we do not provide these here.)

Table 2 presents a selection of the performance comparison results for models **P8–P12** when $N_1 = N_2 = 25$. (The results for all tests with $N_1 = N_2 = 10$ replicates are also shown in Table S8, Appendix D.2.) As expected, the ANT performs extremely well in all these studies since the underlying assumptions of the methodology are adhered to. Nevertheless, it is encouraging that the WST, FT and HT also all have an empirical power over 95% (25 replicates) showing that our methodology can also be successfully applied to functional time series as designed for the ANT. However, the HFT had difficulty discriminating between groups when the period difference was less than 2 hours. This was no surprise as the HFT was constructed to detect differences in scale only and, due to the lower frequency resolution of the wavelet spectrum, the total power within each scale of the wavelet spectrum will be very similar for both groups.

4.1.2. *Power comparisons: Conclusions.* In practice, the suitability of the testing procedures is determined by a combination of factors, such as the practical problem posed by scientists, the degree to which the data adheres to the underlying theoretical assumptions and the number of available replicates. For exam-

Model	Test Group Period	WST (FDR)	FT (FDR)	HFT (FDR)	HT (FDR)	ANT
P8	21	100.0	100.0	100.0	100.0	100.0
P9	22	100.0	100.0	100.0	100.0	100.0
P10	23	100.0	100.0	92.0	100.0	100.0
P11	23.5	100.0	100.0	31.8	100.0	100.0
P12	23.75	100.0	97.9	9.1	98.3	100.0

TABLE 2

Performance Comparison: Simulated power estimates (%) for models P8-P12 with nominal size of 5% with $N_1 = N_2 = 25$ realisations from each group and using the false discovery rate procedure (FDR). Note: Control group period is 24 hours in each model.

ple, models **P1-P3** all stem from a simulated LSW structure and thus would be subject to a test for time-scale equality departure, carried out through an ‘FT’ as its theoretical assumptions are closely adhered to. Recall that the ‘WST’ was proposed as a ‘naive’ variant and is heavily reliant on the number of replicates in order to achieve the appropriate distributional properties, thus its best results are obtained for models that have been simulated from time-varying AR processes. Meanwhile, for data following models that exhibit a gradual period change (such as **P4-P5**) one might be interested in identifying scale-dependent patterns or discrepancies, carried out through the ‘HT’ or ‘HFT’.

4.2. *Size comparisons.* To explore statistical size, we simulate data from a number of models and we assess how often our hypothesis tests reject the null hypothesis of spectral equality (i.e. the time series are generated in the same way for both test groups). The models are denoted **M1-M5** respectively and defined as follows.

1. **M1: Fixed Spectra.** We simulate all data from the wavelet spectrum associated with Group 1 in models **P1**, **P2** and **P3**, which we define as $\{S_j^{(1)}(z)\}_{j=1}^J$ in equation (D.1).
2. **M2: Gradual Period Change.** We simulate all data from the wavelet spectrum which corresponds to a time series that gradually changes period from 24 to 25 hours over (approximately two days), before continuing with period 25 hours for a further two days (i.e. Group 1 from models **P4/P5**).
3. **M3: AR Processes With Abruptly Changing Parameters.** Each time series is generated from the process defined by equation (D.5) with the abruptly changing parameters as defined for group $i = 1$ in Table S4 (i.e. Group 1 from model **P6**).
4. **M4: AR Processes With Slowly Changing Parameters.** Each time series is generated from the process defined by equation (D.6) with the slowly

changing parameters as defined for group $i = 1$ in Table S5 (i.e. Group 1 from model P7).

5. **M5: Functional Time Series (Constant Period).** All data are simulated (using equation (D.7)) from the model that corresponds to a time series with a constant period of 24 hours (i.e. Group 1 from models P8–P12).

4.2.1. *Discussion of findings.* The empirical size values for models M1–M4 with $N_1 = N_2 = 25$ (this is the typical number of available replicates in circadian experiments, see Appendix A) are reported in Table 3. The results for the HFT with $N_1 = N_2 = 1$ are shown in Table S6, Appendix D.2 (recall: the HFT is the only proposed test which can be applied when replicate data is not available—see Section 3.2). The results for all tests with $N_1 = N_2 = 10$ and 50 replicates are shown in Table S9 (Appendix D.2).

These studies show that the empirical size corresponding to all proposed tests (apart from the FT for model M4 with $N_1 = N_2 = 10$ and 25) are less than the nominal size of 5%. A close inspection of rejections for the FT for model M4 with $N_1 = N_2 = 10$ and 25 and both multiple-hypothesis testing methods (Table S10 in Appendix D.2) reveals that, for this particular example, the number of rejections is often 1. If we disregard such situations, the empirical size of the FT also falls below the nominal size of 5% for all sample sizes and multiple-hypothesis testing procedures. In practice, circadian scientists are mostly interested in the numbers of rejections and their locations and often choose to disregard situations where very few coefficients are significantly different. Indeed, this is also our approach in Section 5.

Effect of Sample Size. Note that the tests scale well with increasing sample size, with the nominal size acting as an upper bound, a behaviour also present in other related empirical size investigations, see e.g. Cho (2016).

Approach to Multiple-hypothesis Testing. These studies show that the Bonferroni correction provides a more conservative approach, whereas the false discovery rate (using the correction outlined above) is closer to the nominal size.

Performance Comparison. The results for model M5 with $N_1 = N_2 = 10$ and 25 are shown in Table S8 (Appendix D.2). Note that the empirical size estimates for our proposed tests are all lower than the nominal size of 5%, whereas for 10 replicates the empirical size of the ANT is 7.9%.

4.2.2. *Size comparisons: Conclusions.* These studies show that the empirical size corresponding to all proposed tests is less than the nominal size of 5% (apart from the FT for model M4 with $N_1 = N_2 = 10$ and 25—where, in most cases, the number of significant coefficients was less than 5). We thus recommend using the less conservative FDR procedure (ignoring situations with very small numbers of rejections). Note this also yields better results for empirical power (see

Model	WST (Bon.)	WST (FDR)	FT (Bon.)	FT (FDR)	HFT (Bon.)	HFT (FDR)	HT (Bon.)	HT (FDR)
M1	0.6	1.3	2.5	3.1	0.1	2.0	2.3	2.7
M2	0.3	0.6	3.0	3.9	0.4	3.3	2.5	2.7
M3	0.2	1.5	3.6	3.9	0.0	1.6	3.5	3.8
M4	0.4	0.9	4.6	5.2	1.0	2.4	3.4	3.8

TABLE 3

Simulated size estimates (%) for models M1-M4 with nominal size of 5% and $N_1 = N_2 = 25$ realisations from each group. Empirical size estimates over the nominal size of 5% are highlighted in bold.

Section 4.1.1) whilst also remaining below the nominal size.

4.3. *Sensitivity analysis.* In this section we investigate the sensitivity of our proposed tests to certain modelling assumptions. We investigate: (1) departures from the normality assumption and (2) impact of the choice of wavelet family used within the spectral estimation procedures of each of our proposed tests. Throughout this section, we use $N_1 = N_2 = 25$, since this is the typical number of available replicates in circadian experiments (see Appendix A).

4.3.1. *Departures from Normality.* Recall the proposed statistical testing methodology assumes the innovations $\{\xi_{j,k}\}$ to be normally distributed. To investigate the impact of this assumption, we computationally assess the power and size of the proposed tests within the settings outlined in Section 4 for models **P1–P5** and **M1–M2** but simulated using non-Gaussian innovations (specifically following a t -distribution with 5, and subsequently 3, degrees of freedom). The results can be found in Table S11 (Appendix D.2). Unsurprisingly, when the normality assumption is broken, the empirical power of all tests is less than (or equal to) the empirical power when the innovations follow a standard normal distribution. The increasing distributional departure from normality appears to be of little relevant influence when testing data simulated from models **P1** and **P3** (across all tests), while the empirical power drops for the HT corresponding to models **P2** and **P4/P5**. The testing procedures break for models **P4/P5** with t_3 -distributed innovations, as intuitively, the presence of heavier innovations make the gradual period change structure of models **P4/P5** very difficult to discriminate. We also note that the HT is heavily reliant on the distributional assumptions (see Section 3.3) which explains its sensitivity. Due to its construction (see Section 3.1.2), the FT appears to more readily reject the null hypothesis, increasing the empirical size of the test. However, if we disregard situations where there are a very low number of rejections (see Section 4.2.1) the empirical size of the FT falls below the nominal size of 5% for both multiple-hypothesis testing pro-

cedures and all studies (other than M1 with FDR). We report here that the empirical power of the ANT for model **P1** (fixed spectra) with t -distributions with 5 degrees of freedom was 6.8%, which is below the results in Table S11 for all our proposed tests (which are all over 99.9%). This is to be expected since, as in Section 4.1, the underlying assumptions of the ANT are not valid. (Similar results are obtained for models **P2–P7**, hence we do not provide these here.)

We also investigated the power and size for models **P8–P12** and **M5** (see Section 4) simulated using non-Gaussian errors (specifically following t -distributions with 5, and subsequently 3, degrees of freedom). The results can be found in Table S12 (Appendix D.2). The WST, FT and HT appear to share a good degree of robustness as they all have an empirical power over 99% for models **P8–P11**, showing that our methodology can also be successfully applied to functional time series (as designed for the ANT) with non-Gaussian error. Akin to the previous results for the gradual period change models **P4/P5**, the distribution of the noise term does appear to have an adverse effect in model **P12**, where the difference between the periods of the two underlying signals is only 15 minutes. Across this study, the HFT was most affected. A possible explanation is that the HFT was constructed to detect differences in scale only and, due to the lower frequency resolution of the wavelet spectrum, the total power within each scale of the wavelet spectrum will be very similar for both groups. This issue will have been compounded by the heavier tailed distribution of the noise term. We also report here that, in the settings of this study, the performance of ANT was sustained as its underlying assumptions are adhered to.

4.3.2. Choice of wavelet. The wavelet system gives a representation for non-stationary time series under which we estimate the wavelet spectrum and subsequently perform hypothesis testing. We investigated the sensitivity of our methods to the wavelet choice. For models **P1–P5**, the Haar wavelet was used for spectral estimation, but different, potentially mismatched wavelets were used to generate the processes from the spectrum: Haar wavelets, Daubechies' least-asymmetric wavelets with 4 vanishing moments and Daubechies' extremal phase wavelets with 10 vanishing moments. Models **P6–P12** were not generated from LSW spectra (see Section 4), hence we report the results when using a selection of wavelets for the empirical wavelet spectrum.

The results in Tables S13 and S14 (Appendix D.2) show that our methodology is fairly robust to the wavelet choice. The empirical size estimates all fall below the nominal size. The results indeed support the intuition that, as the scope of our work is to devise tests that locally identify dissimilarities between pairs of spectra, the short support overlaps of Haar wavelets counterbalance their otherwise reduced capacity of representing smooth signals.

4.4. *Summary of findings.* A summary of the hypothesis tests developed in this manuscript detailing the test name, its acronym, strengths and weaknesses can be found in Table S15 (Appendix E).

5. Real data analysis: back to the motivating circadian datasets. We now use our proposed methodology to analyse the motivating examples (Section 1). Prior to analysis, we investigate whether the normality assumption is tenable for each of our motivating datasets. The results (Appendix B.2) show that, for each of our motivating datasets, the normality assumption is appropriate. We then model each circadian trace as a (Gaussian) LSW process, estimate its corresponding group wavelet spectral representation and consequently construct the appropriate test statistic that aims to identify whether a departure towards a specific type of spectral difference is present or not (as described in Section 3). For each dataset, the corresponding number of rejections can be found in Table S3 (Appendix B.1), with corresponding representative ‘barcode’ plots in Figures 4, 5 and 6.

We also note here that the data naturally shared the same starting point and had the same length (see Appendix A). Therefore, instances where these conditions are not satisfied are not the focus of this paper and we leave these issues for future research.

5.1. *Lead dataset.* Section 1.1.1 outlined the scientific aims to determine if lead nitrate affects the circadian clock and, if so, to detect the times and scales at which any significant differences arise between the ‘Control’ and ‘Lead’ exposure groups. Therefore we are particularly interested in the results of the FT. Table S3 shows the results for the FT and includes both the more conservative Bonferroni correction and FDR. In order to visualise the areas of null hypothesis rejection of spectral equality between the control and lead-exposure groups, both group average estimated spectra as well as the ‘barcode’ plot for the FT (with FDR) appear in Figure 4. Figure 4 indicates that the differences between the two spectra lie in resolution levels 2–4, directly corresponding to a circadian rhythm, with the number of rejections increasing with exposure time. We conclude that there is evidence that exposure to lead does affect the circadian clock of *A. thaliana*, and this change manifests itself after approximately three days of free-running conditions.

5.2. *Ultradian dataset.* Section 1.1.2 introduced this experiment and highlighted the need to detect whether any differences appear in the circadian and ultradian components of the ‘Control’ and ‘Mutant’ groups. Hence we are interested in the results of the HFT, specifically developed to identify the scales, rather than the times, at which potential differences arise. Table S3 shows the

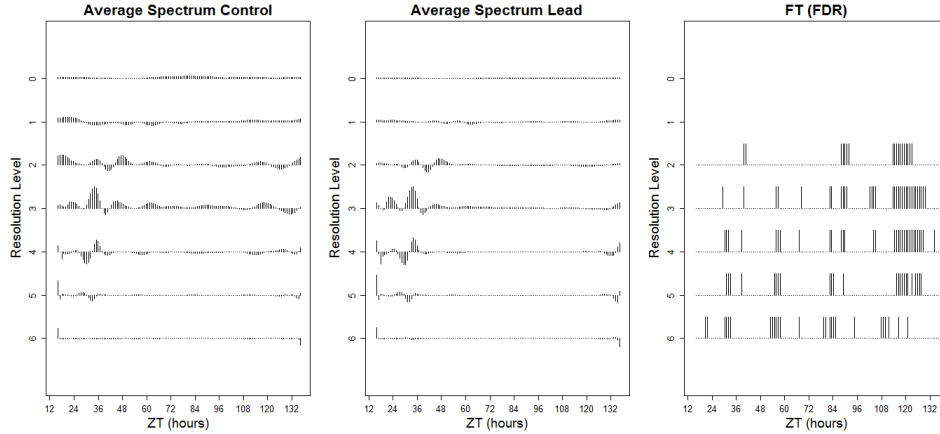


FIG 4. **Lead dataset.** Left: Average estimated spectrum of the ‘Control’ group; Centre: Average estimated spectrum of the ‘Lead’ group; Right: ‘Barcode’ plot for FT (with FDR).

results for the HFT, including both the Bonferroni correction and FDR. The results indicate rejections of the null hypothesis of spectral equality between the control and mutant plants across a range of scales. The group average estimated spectra and ‘barcode’ plot for the HFT (with FDR) can be found in Figure 5. Note that the differences between the two spectra lie in the coarsest resolution levels 1–4, associated with circadian rhythms, and higher-frequency levels 6 and 7, corresponding to an ultradian rhythm. We conclude that there is evidence that the mutant plants have altered circadian and ultradian rhythms within *A. thaliana*.

5.3. *Nematode dataset.* The experiment in Section 1.1.3 aimed to elucidate the effect of a pharmacological treatment on the *C. elegans* clock. The average estimated spectra of the ‘Control’ and ‘Treatment’ groups in Figure 6 share a common profile but with differences in magnitude, indicating that the HT would be appropriate in this context. Table S3 shows that the HT found no significant difference between the shapes of the two spectra, but when tested for equality, the FT (with FDR) found multiple rejections of the null hypothesis of spectral equality between the ‘Control’ and ‘Treatment’ groups (refer to the ‘barcode’ plot in Figure 6). This provides evidence that the two spectra have the same profile within each scale up to an additive non-zero constant. We thus conclude that there is evidence that the treatment significantly affects the intensity of the spectral behaviour, but not its pattern. The spectral differences are present at the highest frequencies (resolution levels 6–8) as an early response to the onset of treatment (prior to time $T = 48$), see Figure 6.

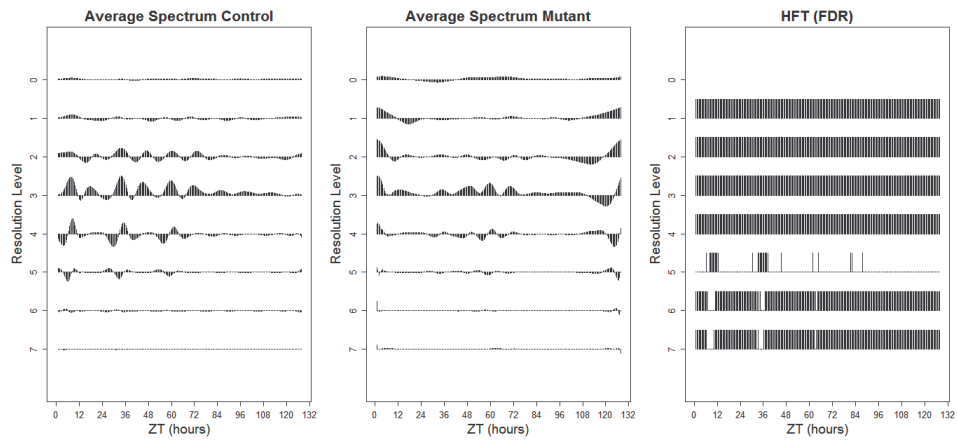


FIG 5. *Ultradian dataset*. Left: Average estimated spectrum of the 'Control' group; Centre: Average estimated spectrum of the 'Mutant' group; Right: 'Barcode' plot for HFT (with FDR).

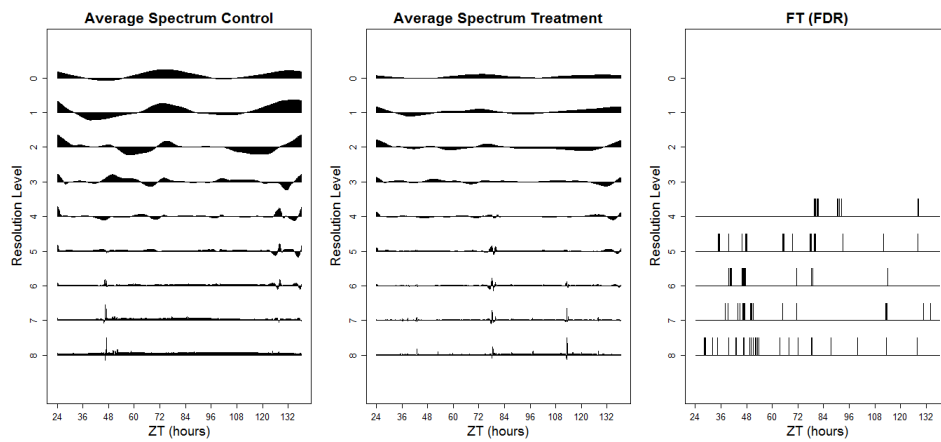


FIG 6. *Nematode dataset*. Left: Average estimated spectrum of the 'Control' group; Centre: Average estimated spectrum of the 'Treatment' group; Right: 'Barcode' plot for FT (with FDR).

5.4. *Discussion of results.* Overall, we recall that, for each of our motivating datasets, the established Fourier-based tests currently adopted within the circadian community found no significant difference between the groups (see Table S1 in Appendix B.1), even though qualitative differences are easily noted (see Section 1.1). This methodology assumes data stationarity, but for our motivating datasets we have shown that this assumption is not appropriate (see Table S2 in Appendix B.1). Our proposed methodology was able to detect the visually apparent differences between the motivating datasets when the current methodology could not (see Tables S3 and S1 in Appendix B.1). Due to the nonstationary character of the proposed approach, it also additionally indicates precise times and/or scales at which differences become manifest.

6. Conclusions and further work. This work was stimulated by a variety of challenging applications faced by the circadian–biology community, which is becoming increasingly aware of the nonstationary characteristics present in much of their data (Hargreaves et al., 2018; Zielinski et al., 2014; Leise et al., 2013). Our methodology fills the gap in the current literature by developing and testing much needed tools for the formal spectral comparison of nonstationary data. Our methods are developed as testing procedures, analogous to the period analysis techniques currently adopted within the circadian community. Motivated by three complementary applications in circadian biology, our new methodology allows the identification of three specific types of spectral difference. Table S15 in Appendix E provides a summary of the hypothesis tests developed in this manuscript detailing their strengths and weaknesses.

The competitive performance of our methods was comparatively assessed in an extensive simulation study (Section 4). Additionally, when compared to existing methods currently adopted within the circadian community, our proposed tests were able to discriminate between real data sets (Table S3) where the current methodology could not (Table S1).

In the applications provided, we illustrated the important implications in further understanding the mechanisms behind the plant and nematode circadian clocks, and the environmental implications associated with soil pollution. However, we note that our methodology can readily be applied to other circadian datasets, as well as to data originating in other fields, as long as the data share the same dyadic length (T). This assumption is easily achievable for most experimental data, but for other setups might necessitate further specific treatments depending on the discrepancy between the number of observations.

In all of our proposed hypothesis tests, we wish to test many hypotheses of the type $H_0 : S_j^{(1)}(k/T) = S_j^{(2)}(k/T)$ for several values of j and k . In this manuscript we tested the Bonferroni correction and, for a less conservative approach, the

false discovery rate (FDR) procedure. We recommend the use of the FDR procedure, as this gave a higher empirical power and was closer to the nominal size in the simulation studies (see Section 4). However, the multiple-hypothesis testing methods we use do not account for the dependence of the spectral coefficients. The hypothesis tests developed in Sections 3.2 and 3.3 alleviate this problem by transforming the data to produce coefficients that are approximately uncorrelated but, as neither method fully decorrelates the data, multiple-hypothesis testing methods that take the dependence of the (transformed) spectral coefficients into account are an interesting avenue of further work.

APPENDIX A: EXPERIMENTAL DETAILS

In this section we outline the experimental details that led to the datasets introduced in Section 1.1 and subsequently analysed in Sections 5.1, 5.2 and 5.3. *Experimental overview: Lead and Ultradian Datasets.* Both Davis and Millar labs used a firefly luciferase reporter system. This involves fusing the gene of interest (here, ‘cold and circadian regulated and RNA binding 2’, *CCR2*) to a bioluminescent enzyme called luciferase (Doyle et al., 2002). When *CCR2* is expressed, the resultant luciferase emits light which is measured using a TopCount NXT scintillation counter (Perkin Elmer), allowing relative gene expression of *CCR2* to be quantified *in vivo* (Southern and Millar, 2005; Perea-García et al., 2015).

Lead nitrate dataset. *Arabidopsis thaliana* seeds (Ws-*CCR2:LUC* (Doyle et al., 2002)) were surface sterilised and plated onto Hoagland’s media containing 1% sucrose, 1.5% phyto agar (Hoagland et al., 1950). The seeds were stratified for 2 days at 4°C and transferred to growth chambers to entrain under 12:12 light/dark cycles at a constant temperature of 20°C. Six-day-old seedlings were transferred to 96 well microtiter plates containing Hoagland’s 1% sucrose, 1.5% agar (Hanano et al., 2006) with or without supplemental $\text{Pb}(\text{NO}_3)_2$ (lead nitrate) at a concentration of 1.4mM. After 24 hours, the plants were then transferred to the TOP-Count machine. Measurements were taken at intervals of approximately 45 minutes. Measurement began after the transition to 12 hours of darkness (known as subjective dusk) on the seventh day of the plants’ life. Therefore, the plants experience one ‘normal’ day in the TOPCount machine (known as entrainment). After this, the plants are exposed to constant light (known as an LL free-run) for approximately four days. This dataset consists of 48 plant signals recorded at $T = 128$ time points, with both the ‘Control’ and ‘Lead’ groups containing 24 plants.

Ultradian dataset. (Millar et al., 2015). This dataset was obtained following a similar method as outlined for the Lead dataset above, but compared ‘Control’ *A. thaliana* plants (Ws-2 with *CCR2:LUC* (Doyle et al., 2002)) with ‘Mutant’ *A. thaliana* plants (Ws-2 *cca1 lhy*). Plants were grown on MS media Murashige and

Dataset	Mean Period Estimate: Control Group	Mean Period Estimate: Test Group	Difference	p-value
Lead	27.4	26.8	-0.6	0.16
Ultradian	6.5	6.5	0.0	0.98
Nematode	24.8	25.6	+0.8	0.55

TABLE S1

A summary of the output of the analysis of the motivating example datasets in BRASS: the mean period estimate for the control and test groups in hours (obtained using FFT-NLLS analysis (Plautz et al., 1997)), the difference between the period estimates and the corresponding p-value.

Skoog (1962) with 3% sucrose and 1.5% phyto-agar. Plants were entrained in 12:12 L:D conditions at 22°C followed by an LL free-run. Measurements were taken at intervals of approximately 30 minutes. This dataset consists of 48 plant signals recorded at $T = 256$ time points, with both the ‘Control’ and ‘Mutant’ groups containing 24 plants.

Nematode dataset. This dataset was obtained using male *Caenorhabditis elegans* strain PE254 (obtained from the CGC), which expresses firefly luciferase under the promoter of the *sur-5* gene (*fels4 [P_{sur-5}::luc+::gfp; rol-6(su1006)]*) (Lagido et al. (2008)). Nematodes expressing luciferase driven by the *sur-5* promoter have previously been reported to show circadian rhythms in luminescence (Goya et al., 2016). Single nematodes were placed in wells containing 100µl S buffer (Stiernagle, 1999), supplemented with 5 mg/mL cholesterol, 1 g/L wet weight pelleted *Escherichia coli* OP50 strain and 100 µM luciferin. Treatment wells also contained 10 µM SB 203580 (a p38 MAPK inhibitor (Sigma S8307)). Entrainment conditions were 12 hours at 20°C followed by 12 hours at 15°C for two days in constant darkness. Free-running was at 20°C in constant darkness. Luciferase measurements were recorded approximately every 13 minutes. Nematodes that died (shown by a sudden loss of luciferase expression) were excluded from data analysis. Therefore, this dataset consists of 62 signals recorded at $T = 512$ time points, with the ‘Control’ and ‘Treatment’ groups containing 32 and 30 time series respectively.

APPENDIX B: REAL DATA ANALYSIS: SUPPLEMENTARY MATERIAL

B.1. Supplementary Tables. In this section, for each motivating example dataset, we report: a summary of the output of the analysis of the motivating datasets in BRASS (Table S1); the results of the Priestley-Subba Rao test of stationarity (for each time series) in Table S2 and the number of rejections for the relevant proposed hypothesis testing procedure (Table S3).

Dataset	Lead	Ultradian	Nematode
Number of nonstationary time series	39 (81%)	41 (85%)	61 (98%)
Total number of time series	48	48	62

TABLE S2

Results for the Priestley-Subba Rao test of stationarity, implemented in the `fractal` package in `R` and available from the CRAN package repository. Number of nonstationary plants indicates the number of time series (in each motivating example dataset) with enough evidence to reject the null hypothesis of stationarity at the 5% significance level (as a percentage in brackets).

Dataset (Test)	Bon.	FDR
Lead (FT)	31 (3%)	133 (15%)
Ultradian (HFT)	1102 (54%)	1538 (75%)
Nematode (HT)	0 (0%)	0 (0%)

TABLE S3

The number of rejections (as a percentage in brackets) for each relevant proposed test and multiple-hypothesis testing procedure for the motivating example datasets.

B.2. Tenability of the Normality Assumption. In this section we investigate the tenability of the normality assumption for each of our motivating datasets. Following Fryzlewicz (2005), for each series, we standardise the (zero-mean) data using an estimate of the local standard deviation. The estimate was obtained by means of a localised a Gaussian kernel with bandwidth chosen using the methods of Fryzlewicz (2005). We then examine the Q–Q plot of the standardised series against the normal quantiles. We report Q–Q plots for a representative series from the control and test groups of each of our motivating datasets in Figure S1. These demonstrate that the normality assumption holds for our motivating data, an assumption also typically undertaken by the circadian community (Perea-García et al., 2015).

APPENDIX C: BACKGROUND FOR LOCALLY STATIONARY WAVELET (LSW) PROCESSES

In this section we provide the technical details that underline the LSW process model introduced by Nason et al. (2000).

The locally stationary wavelet processes are a sequence of doubly indexed stochastic processes $\{X_{t,T}\}_{t=0,\dots,T-1}$, $T = 2^J \geq 1$, having the representation in the mean-square sense

$$(C.1) \quad X_{t,T} = \sum_{j=1}^J \sum_k w_{j,k;T} \psi_{j,k}(t) \xi_{j,k},$$

where $\xi_{j,k}$ is a random orthonormal increment sequence and where $\{\psi_{j,k}(t)\}_{j,k}$

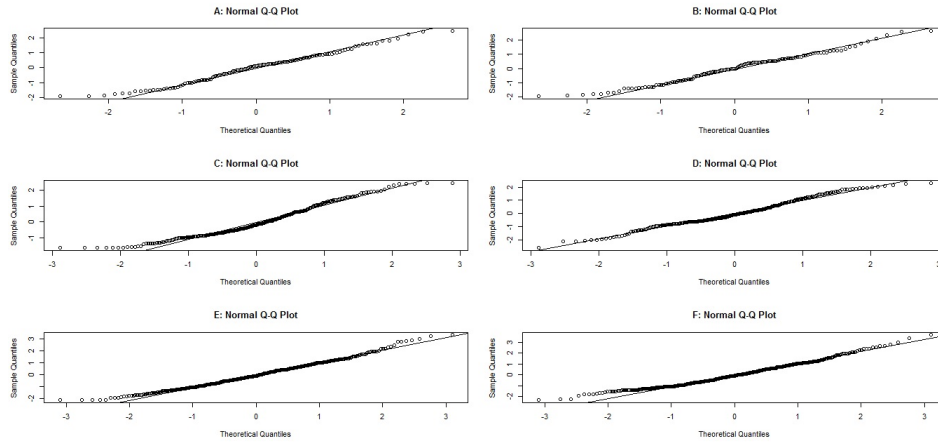


FIG S1. Q-Q plots for a representative series from the control (Plots A, C, E) and test groups (Plots B, D, F) of each of our motivating datasets. Lead Dataset: Plots A and B. Ultradian Dataset: C and D. Nematode Dataset: E and F

is a discrete non-decimated family of wavelets based on a mother wavelet $\psi(t)$ of compact support. The quantities in equation (C.1) have the following properties:

- (a) $\mathbb{E}(\xi_{j,k}) = 0$ for all j, k . Hence $E(X_{t,T}) = 0$ for all t, T ,
- (b) $\text{Cov}(\xi_{j,k}, \xi_{\ell,m}) = \delta_{j,\ell} \delta_{k,m}$ where $\delta_{i,j}$ is the Kronecker delta.
- (c) There exists, for each $j \geq 1$ a Lipschitz continuous function $W_j(z)$ for $z \in (0, 1)$ which fulfils the following properties:

$$\sum_{j=1}^{\infty} |W_j(z)|^2 < \infty \quad \text{uniformly in } z \in (0, 1);$$

the Lipschitz constants L_j are uniformly bounded in j and

$$\sum_{j=1}^{\infty} 2^j L_j < \infty;$$

there exists a sequence of constant C_j such that for each T

$$\sup_k |w_{j,k;T} - W_j(k/T)| \leq C_j / T,$$

where $\{C_j\}$ fulfils $\sum_{j=1}^{\infty} C_j < \infty$.

The (evolutionary) wavelet spectrum is defined as $S_j(z) = |W_j(z)|^2$ at scale j and rescaled time $z = t/T$, and is connected to a localised autocovariance function defined for each (rescaled) time z and lag τ as follows

$$(C.2) \quad c(z, \tau) = \sum_{j=1}^{\infty} S_j(z) \Psi_j(\tau).$$

In the above, the quantities $\{\Psi_j(\tau)\}_j$ define a family of locally supported auto-correlation wavelets that can deliver sparse representations (Nason et al., 2000). Once a well-behaved spectral estimator has been obtained, equation C.2 can be used to obtain a local autocovariance estimator $\hat{c}(z, \tau)$ and its approximate confidence bounds, under the assumption of Gaussian innovations (Nason, 2013).

APPENDIX D: DETAILED DESCRIPTION OF SIMULATION STUDIES

In this section we give a more detailed description of the simulation studies outlined in Section 4. The basic structure of each simulated experiment can be described as follows. In each case, we assumed that the signal was a realisation of length $T = 256$ from one of $i = 1, 2$ possible groups, each having (possibly) different spectral structure. A set of $N_1 = N_2 = 1, 10, 25, 50$ signal realisations for each group was generated either from variously defined: spectra (models **P1–P5** and **M1** and **M2**); AR processes (models **P6, P7, M3** and **M4**) or functional time series (models **P8–P12** and **M5**).

For the models defined by group spectra, signal realisations were generated using the `locits` package in R (available from the CRAN package repository) and the representation in equation (2.2) with (unless otherwise stated) the Haar wavelet and a Gaussian orthonormal increment sequence with mean zero and unit variance. (Note that the `wavethresh` package in R preceded the `locits` package and can also be used to generate LSW processes. For more information on how to generate LSW processes from a particular spectrum see Nason (2010).)

D.1. Model Details. In this section we give a detailed description of each model outlined in Sections 4.1 and 4.2.

1. **P1: Fixed Spectra.** We follow Krzemieniewska et al. (2014) Section 4.1.1-Fixed spectra where the spectra of the two groups differ only at the finest level by 100 coefficients. We simulate each replicate r_i -th time series of length $T = 256$ of the i -th group from the wavelet spectrum $\{S_j^{(i)}(z)\}_{j=1}^J$ which we define for each of the $i = 1, 2$ groups as follows:

$$(D.1) \quad S_j^{(1)}(z) = \begin{cases} 4 \cos^2(2\pi z), & \text{for } j = 3, z \in (0, 1) \\ 1, & \text{for } j = 7, z \in (1/256, 56/256) \\ 0, & \text{otherwise;} \end{cases}$$

and

$$(D.2) \quad S_j^{(2)}(z) = \begin{cases} 4 \cos^2(2\pi z), & \text{for } j = 3, z \in (0, 1) \\ 1, & \text{for } j = 7, z \in (1/256, 156/256) \\ 0, & \text{otherwise.} \end{cases}$$

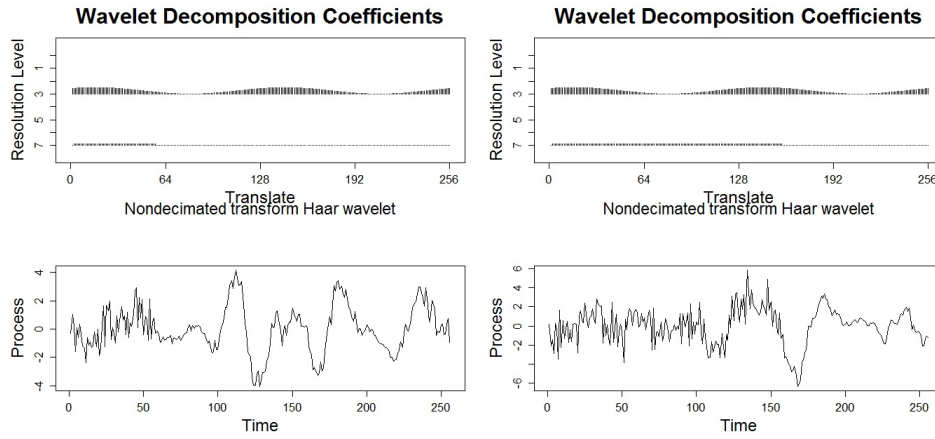


FIG S2. **P1: Fixed Spectra.** Top left: Group 1 wavelet spectrum; Top right: Group 2 wavelet spectrum; Bottom left: Group 1 realisation; Bottom right: Group 2 realisation.

Figure S2 provides a visualisation of the wavelet spectra (top row) and an example of a signal realisation from each of the two groups (bottom row).

2. **P2: Fixed Spectra-Fine Difference.** For our next study, we modify the setting above such that the spectra of the two groups differ by 6 coefficients (in resolution level 7). Therefore, $\{S_j^{(1)}(z)\}_{j=1}^J$ is as defined in equation (D.1) above but we specify the evolutionary wavelet spectrum $\{S_j^{(2)}(z)\}_{j=1}^J$ as follows:

$$(D.3) \quad S_j^{(2)}(z) = \begin{cases} 4 \cos^2(2\pi z), & \text{for } j = 3, z \in (0, 1) \\ 1, & \text{for } j = 7, z \in (1/256, 50/256) \\ 0, & \text{otherwise.} \end{cases}$$

Figure S3 provides a visualisation of the wavelet spectra (top row) and an example of a signal realisation from each of the two groups (bottom row).

3. **P3: Fixed Spectra-Plus Constant.** We now define fixed spectra such that the spectra of the two groups differ by a constant at the finest resolution level. Therefore, $\{S_j^{(1)}(z)\}_{j=1}^J$ is as defined in equation (D.1) above but we specify the evolutionary wavelet spectrum $\{S_j^{(2)}(z)\}_{j=1}^J$ as follows:

$$(D.4) \quad S_j^{(2)}(z) = \begin{cases} 4 \cos^2(2\pi z), & \text{for } j = 3, z \in (0, 1) \\ 2, & \text{for } j = 7, z \in (1/256, 56/256) \\ 1, & \text{for } j = 7, z \in (57/256, 256/256) \\ 0, & \text{otherwise.} \end{cases}$$

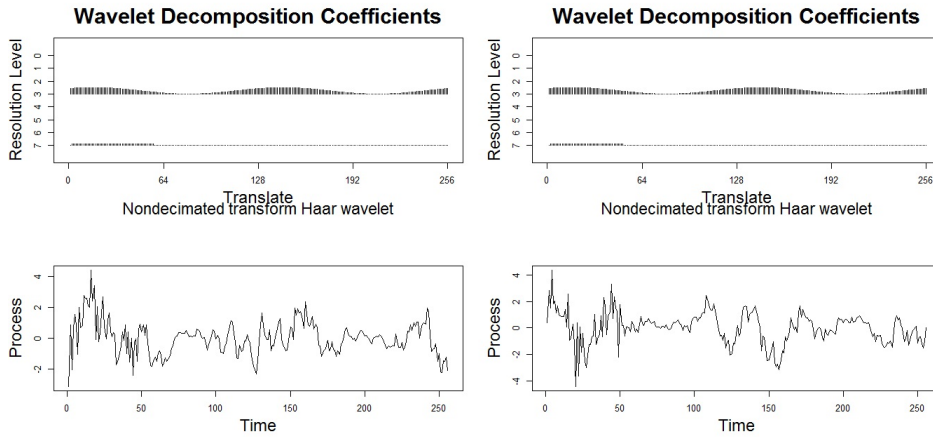


FIG S3. **P2:Fixed Spectra-Fine Difference.** Top left: Group 1 wavelet spectrum; Top right: Group 2 wavelet spectrum; Bottom left: Group 1 realisation; Bottom right: Group 2 realisation.

Figure S4 provides a visualisation of the wavelet spectra (top row) and an example of a signal realisation from each of the two groups.

4. **P4/P5: Gradual Period Change.** With this simulation study aiming to replicate a typical circadian experiment with changes beyond the stationarity assumption, we define time series as realisations from one of 3 possible groups, each with different spectral characteristics. In particular, each group represents a time series that gradually changes period from 24 to: 25 (Group 1), 26 (Group 2) and 27 (Group 3) over (approximately) two days, before continuing with the relevant period for a further two days. We choose $T = 256$ which is equivalent to a free-running period of 4 days with equally spaced observations every 22.5 minutes. Figure S5 shows the wavelet spectra which display the gradually changing periods that define each of the 3 groups. (Note that the increased period is shown by the movement up through the resolution levels and the gradual increase in period of the wavelet coefficients.) To determine which changes can be discriminated by the methods, we perform two studies within this setting: **P4**: simulations from Group 1 and Group 2 and **P5**: simulations from Group 1 and Group 3.
5. **P6/P7: AR Processes with Time-Varying Coefficients.** The signals in models **P1–P5** are generated from a defined group spectrum, satisfying the underlying LSW modelling assumptions of our proposed tests. The purpose of this study is to assess the performance of our tests when these assumptions are not met. Therefore, we simulate from an important class

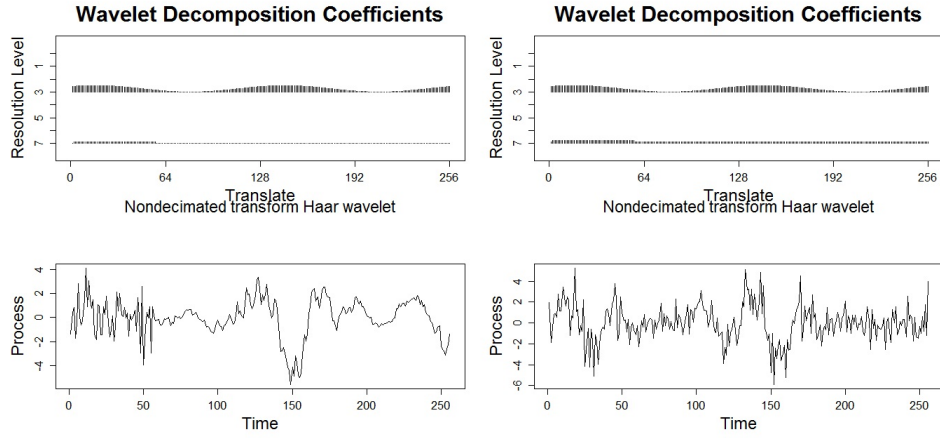


FIG S4. **P3:Fixed Spectra-Plus Constant.** Top left: Group 1 wavelet spectrum; Top right: Group 2 wavelet spectrum; Bottom left: Group 1 realisation; Bottom right: Group 2 realisation.

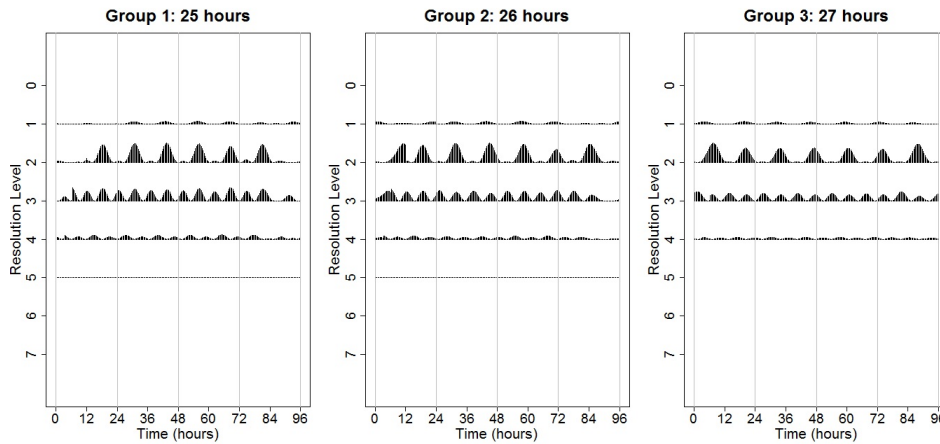


FIG S5. **P4/P5: Gradual Period Change.** Left: Group 1 wavelet spectrum (gradual period change from 24 to 25 hours); Centre: Group 2 wavelet spectrum (gradual period change from 24 to 26 hours); Right: Group 3 wavelet spectrum (gradual period change from 24 to 27 hours).

Time-varying parameters	Time Index	Group $i = 1$	Group $i = 2$
$\phi_1^{(i)}(t)$	$t = 1, \dots, 53$	0.8	0.8
	$t = 54, \dots, 128$	-0.9	-0.3
	$t = 129, \dots, 256$	0.8	0.8
$\phi_2^{(i)}(t)$	$t = 1, \dots, 256$	-0.81	-0.81

TABLE S4

P6: AR Processes with Abruptly Changing Parameters. The abruptly changing parameters of two nonstationary autoregressive processes.

of nonstationary processes– AR processes with time-varying coefficients. We propose a simulation study in a setting as described in [Fryzlewicz and Ombao \(2009\)](#) Section 4.1 Cases 1 and 2.

P6: AR Processes with Abruptly Changing Parameters. The r_i -th time series from group $i = 1, 2$, denoted $X_{n,t}^{(i),r_i}$ is generated from the process defined by:

$$(D.5) \quad X_t^{(i),r_i} = \phi_1^{(i)}(t)X_{t-1}^{(i),r_i} + \phi_2^{(i)}(t)X_{t-2}^{(i),r_i} + \epsilon_t^{(i),r_i},$$

where the innovations $\epsilon_t^{(i),r_i}$ are independent and identically distributed (iid) Gaussian with zero mean and unit variance. In this study, the squared difference between the group spectra is relatively small and the abruptly changing parameters for the two groups are shown in Table S4. Representative time series plots from each group and the estimated spectra are shown in Figure S6.

P7: AR Processes With Slowly Changing Parameters. The r_i -th time series from group $i = 1, 2$, denoted $X_t^{(i),r_i}$ is generated from the process defined by:

$$(D.6) \quad X_t^{(i),r_i} = \phi_1^{(i)}(t)X_{t-1}^{(i),r_i} + \phi_2^{(i)}(t)X_{t-2}^{(i),r_i} + \epsilon_t^{(i),r_i},$$

where the innovations $\epsilon_t^{(i),r_i}$ are iid Gaussian with zero mean and unit variance. In this study, the group wavelet spectra are highly similar and hence the squared difference between group spectra is relatively small. The slowly changing parameters for groups $i = 1, 2$ are shown in Table S5. Representative time series plots from each group and the estimated spectra are shown in Figure S7.

- P8–P12: Functional Time Series (Constant Period).** This study follows [Zielinski et al. \(2014\)](#) and generates each time series using an underlying cosine curve with additive noise, which also coincides with the theoretical assumptions of the ANT. As in Models **P4** and **P5**, we choose $T = 256$, which is equivalent to a free-running period of 4 days with equally spaced

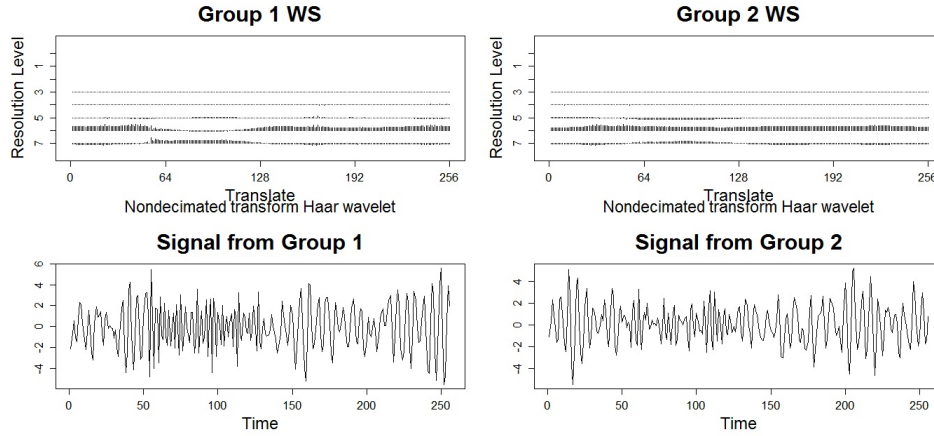


FIG S6. **P6: AR Processes with Abruptly Changing Parameters.** Nonstationary autoregressive processes. Top left: Estimated wavelet spectrum of Group 1; Top right: Estimated wavelet spectrum of Group 2; Bottom left: Group 1 realisation; Bottom right: Group 2 realisation.

Time-varying parameters	Group $i = 1$	Group $i = 2$
$\phi_1^{(i)}(t)$	$-0.8[1 - 0.7 \cos(\pi t/T)]$	$-0.8[1 - 0.1 \cos(\pi t/T)]$
$\phi_2^{(i)}(t)$	-0.81	-0.81

TABLE S5

P7: AR Processes With Slowly Changing Parameters. The slowly changing parameters of two nonstationary autoregressive processes.

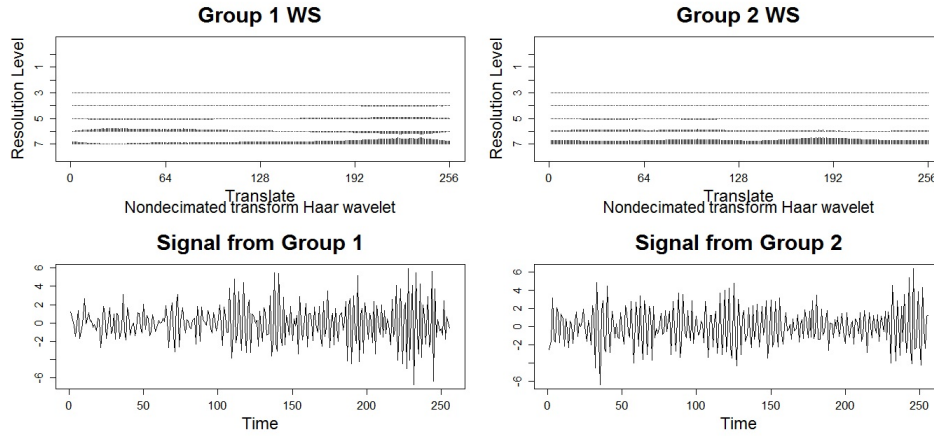


FIG S7. **P7: AR Processes with Slowly Changing Parameters.** Top left: Estimated wavelet spectrum of Group 1; Top right: Estimated wavelet spectrum of Group 2; Bottom left: Group 1 realisation; Bottom right: Group 2 realisation.

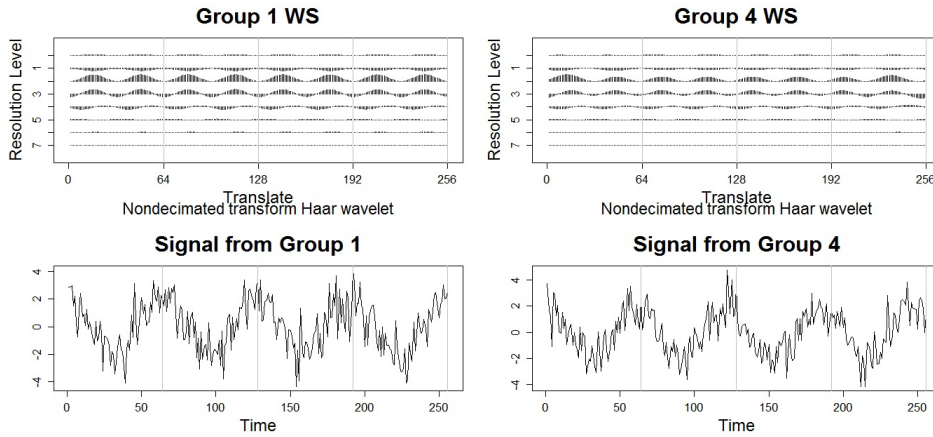


FIG S8. **P10: Functional Time Series with Constant Period.** Top left: Estimated wavelet spectrum of Group 1 (24 hour period); Top right: Estimated wavelet spectrum of Group 4 (23 hour period); Bottom left: Group 1 realisation; Bottom right: Group 4 realisation. Grey lines indicate a 24 hour period.

observations every 22.5 minutes. The r_i -th time series from group $i = 1, 2$, denoted $X_t^{(i),r_i}$ is generated from the process defined by:

$$(D.7) \quad X_t^{(i),r_i} = f^{(i)}(t) + \epsilon_t^{(i),r_i},$$

where the random variables $\epsilon_t^{(i),r_i}$ are iid Gaussian with zero mean and unit variance and the functions $f^{(i)}(t)$ are defined below. We define time series as realisations from one of 6 possible groups, each with a different (constant) period. The function $f^{(i)}(t)$ is set as a cosine curve with an amplitude of 2 and a period of: 24 hours (Group 1), 21 hours (Group 2), 22 hours (Group 3), 23 hours (Group 4), 23.5 hours (Group 5) and 23.75 hours (Group 6). Representative time series plots and the estimated spectra for Groups 1 and 4 are shown in Figure S8. To determine which period changes can be discriminated by the methods, we perform five studies within this setting: simulations from Group 1 and Groups 2–6 (models **P8–P12** respectively).

D.2. Supplementary Tables. In this section we provide results which support the discussion of the hypothesis tests in Section 4. We report the simulated power and size estimates for $N_1 = N_2 = 1, 10, 50$ for the simulation studies outlined in Sections 4.1 and 4.2 in tables S6 – S9. Additionally, we report the number of rejections for the FT for model **M4** with $N_1 = N_2 = 10$ and 25 and both multiple-hypothesis testing methods in Table S10.

Model	P1	P2	P3	P4	P5	P6	P7	M1	M2	M3	M4
HFT (Bon.)	69.4	3.8	72.6	4.1	51.3	2.5	21.8	2.8	4.1	0.8	1.5
HFT (FDR)	77.7	4.9	79.0	5.4	57.9	15.2	35.9	3.2	4.8	1.7	2.1

TABLE S6

Simulated power and size estimates (%) for the HFT for models P1-P7 and M1-M4 with nominal size of 5% and $N_1 = N_2 = 1$ realisation from each group.

N	Model	WST (Bon.)	WST (FDR)	FT (Bon.)	FT (FDR)	HFT (Bon.)	HFT (FDR)	HT (Bon.)	HT (FDR)
10	P1	100.0	100.0	100.0	100.0	100.0	100.0	100.0	100.0
10	P2	3.5	4.6	51.9	54.3	4.1	6.5	16.9	17.4
10	P3	100.0	100.0	100.0	100.0	100.0	100.0	4.2	4.3
10	P4	0.5	0.6	8.4	10.8	4.8	7.0	50.4	55.4
10	P5	0.4	1.1	22.6	31.0	73.4	80.2	95.8	98.4
10	P6	92.2	99.7	14.7	16.4	3.4	30.7	11.6	12.2
10	P7	99.2	100.0	11.5	12.1	30.0	54.7	75.6	77.4
50	P1	100.0	100.0	100.0	100.0	100.0	100.0	100.0	100.0
50	P2	94.8	97.2	100.0	100.0	87.1	88.5	100.0	100.0
50	P3	100.0	100.0	100.0	100.0	100.0	100.0	5.3	5.3
50	P4	11.8	28.0	96.0	99.0	92.0	94.8	100.0	100.0
50	P5	60.2	86.6	100.0	100.0	100.0	100.0	100.0	100.0
50	P6	100.0	100.0	100.0	100.0	96.7	100.0	99.3	99.8
50	P7	100.0	100.0	99.0	100.0	100.0	100.0	100.0	100.0

TABLE S7

Simulated power estimates (%) for models P1-P7 with nominal size of 5%. $N = N_1 = N_2$ is the number of realisations in each group. Highest empirical power estimates are highlighted in bold.

We also report the simulated power and size estimates for $N_1 = N_2 = 25$ for the simulation studies outlined in: Section 4.3.1 in Tables S11 and S12 and Section 4.3.2 in Tables S13 and S14.

APPENDIX E: SUMMARY TABLE

Table S15 provides a summary of the hypothesis tests developed in this manuscript detailing the test name, its acronym, strengths and weaknesses for each of the proposed tests.

REFERENCES

Atkinson, A. D., Hill, R. R., Pignatiello Jr, J. J., Vining, G. G., White, E. D. and Chicken, E. (2017). Wavelet ANOVA approach to model validation. *Simulation Modelling Practice and Theory*, 78:18–27.

N	Model	Test Group Period	WST (FDR)	FT (FDR)	HFT (FDR)	HT (FDR)	ANT
10	P8	21	100.0	100.0	100.0	100.0	100.0
10	P9	22	100.0	100.0	93.3	100.0	100.0
10	P10	23	100.0	100.0	31.9	100.0	100.0
10	P11	23.5	100	96.1	9.5	99.4	100.0
10	P12	23.75	81.2	14.6	5.6	32.4	100.0
10	M5	24	2.0	2.1	3.1	4.1	7.9
25	M5	24	3.0	2.7	2.7	3.5	4.8

TABLE S8

Simulated size and power estimates (%) for models P8-P12 and M5 with nominal size of 5% and using the false discovery rate procedure (FDR). $N = N_1 = N_2$ is the number of realisations in each group. Note: Control group period is 24 hours in each model.

N	Model	WST (Bon.)	WST (FDR)	FT (Bon.)	FT (FDR)	HFT (Bon.)	HFT (FDR)	HT (Bon.)	HT (FDR)
10	M1	0.3	0.5	2.6	3.3	1.0	2.6	2.5	2.7
10	M2	0.0	0.2	2.4	3.6	2.0	5.0	3.3	3.3
10	M3	0.3	1.2	4.1	4.4	0.2	1.4	1.9	2.1
10	M4	0.4	1.6	5.1	5.6	0.9	1.8	2.1	2.2
50	M1	0.4	1.1	2.4	3.9	0.3	2.4	3.1	3.3
50	M2	0.3	0.6	3.1	3.8	1.4	3.1	2.5	2.6
50	M3	0.5	1.2	4.4	4.8	0.2	2.2	3.9	4.2
50	M4	0.2	1.1	4.4	4.8	1.3	2.6	2.8	2.9

TABLE S9

Simulated size estimates (%) for models M1-M4 with nominal size of 5%. $N = N_1 = N_2$ is the number of realisations in each group. Empirical size estimates over the nominal size of 5% are highlighted in bold.

N	Multiple-hypothesis Testing Method	1 Rej.	2 Rej.	3 Rej.	4 Rej.	>5 Rej.	Modified Empirical Size Estimate
10	Bon.	44	5	2	0	0	0.7
10	FDR	40	12	3	0	1	1.6
25	Bon.	38	8	0	0	0	0.8
25	FDR	31	16	3	2	0	2.1
50	Bon.	39	5	0	0	0	0.5
50	FDR	32	10	3	0	3	1.6

TABLE S10

M4: AR Process with Slowly Changing Parameters. Numbers of rejections in empirical size estimates for the *Raw Periodogram F-Test* (FT), with Bonferroni Correction (Bon.) and false discovery rate (FDR) and with nominal size of 5%. "Modified Empirical Size Estimate" is calculated by examining only cases with more than one significant coefficient.

Model	Test	N(0,1)	t ₅	t ₃
P1	WST	100.0	100.0	100.0
P1	FT	100.0	100.0	100.0
P1	HFT	100.0	99.9	88.4
P1	HT	100.0	100.0	93.3
P2	WST	48.0	30.5	11.6
P2	FT	100.0	100.0	100.0
P2	HFT	31.8	5.6	1.6
P2	HT	86.4	53.5	17.9
P3	WST	100.0	100.0	100.0
P3	FT	100.0	100.0	100.0
P3	HFT	100.0	100.0	97.0
P3	HT	4.4	2.4	1.9
P4	WST	2.7	1.2	0.6
P4	FT	54.5	49.1	35.7
P4	HFT	36.5	4.7	4.0
P4	HT	100.0	79.7	40.0
P5	WST	14.6	1.1	0.3
P5	FT	99.9	76.6	32.9
P5	HFT	100.0	30.1	11.3
P5	HT	100.0	81.6	38.4
M1	WST	1.3	0.7	0.1
M1	FT	3.1	4.1	14.5
M1	HFT	2.0	3.2	1.8
M1	HT	2.7	2.7	0.6
M2	WST	0.6	0.1	0.4
M2	FT	3.9	4.5	4.5
M2	HFT	3.3	2.9	2.1
M2	HT	2.7	0.9	0.9

TABLE S11

Potential Non-Gaussian Innovations: Simulated size and power estimates (%) for models P1-P5 and M1, M2 with nominal size of 5% and $N_1 = N_2 = 25$ realisations from each group. Innovations are distributed as: standard normal (denoted $N(0,1)$) or t-distribution with 5 or 3 degrees of freedom (denoted t_5, t_3 respectively). For the FT, the modified size and power estimates are recorded (i.e. only consider cases when more than 5 rejections are reported– see Section 4.2). Empirical size estimates over the nominal size of 5% are highlighted in bold.

Model	Test	N(0,1)	t_5	t_3
P8	WST	100.0	100.0	100.0
P8	FT	100.0	100.0	100.0
P8	HFT	100.0	100.0	99.6
P8	HT	100.0	100.0	100.0
P9	WST	100.0	100.0	100.0
P9	FT	100.0	100.0	100.0
P9	HFT	100.0	99.9	79.4
P9	HT	100.0	100.0	100.0
P10	WST	100.0	100.0	100.0
P10	FT	100.0	100.0	100.0
P10	HFT	92.0	59.5	25.6
P10	HT	100.0	100.0	100.0
P11	WST	100.0	100.0	100.0
P11	FT	100.0	100.0	100.0
P11	HFT	31.8	15.1	8.1
P11	HT	100.0	100.0	99.5
P12	WST	100.0	98.5	52.4
P12	FT	97.9	83.6	80.0
P12	HFT	9.1	5.9	3.6
P12	HT	98.3	77.2	31.6
M5	WST	3.0	1.0	1.5
M5	FT	2.7	1.7	10.4
M5	HFT	2.7	2.0	0.9
M5	HT	3.5	4.2	1.5

TABLE S12

Potential Non-Gaussian Errors: Simulated size and power estimates (%) for models P8-P12 and M5 with nominal size of 5% and $N_1 = N_2 = 25$ realisations from each group. The noise term in equation (D.7) is distributed as: standard normal (denoted $N(0,1)$) or t -distribution with 5 or 3 degrees of freedom (denoted t_5 , t_3 respectively). For the FT, the modified size and power estimates are recorded (i.e. only consider cases when more than 5 rejections are reported– see Section 4.2).

Empirical size estimates over the nominal size of 5% are highlighted in bold.

Model	Test	Haar wavelet (1 V.M.)	Daubechies' least-asymmetric (4 V.M.)	Daubechies' extremal phase (10 V.M.)
P1	WST	100.0	100.0	100.0
P1	FT	100.0	100.0	100.0
P1	HFT	100.0	100.0	100.0
P1	HT	100.0	100.0	100.0
P2	WST	48.0	55.7	44.6
P2	FT	100.0	100.0	100.0
P2	HFT	31.8	78.2	73.9
P2	HT	86.4	99.9	99.6
P3	WST	100.0	100.0	100.0
P3	FT	100.0	100.0	100.0
P3	HFT	100.0	100.0	100.0
P3	HT	4.4	4.2	6.0
P4	WST	2.7	23.5	25.1
P4	FT	54.5	91.9	89.4
P4	HFT	36.5	96.5	78.0
P4	HT	100.0	50.8	12.3
P5	WST	14.6	55.3	68.0
P5	FT	99.9	98.6	100.0
P5	HFT	100.0	74.7	99.8
P5	HT	100.0	36.5	52.6
M1	WST	1.3	0.3	0.2
M1	FT	3.1	2.5	2.9
M1	HFT	2.0	2.0	1.6
M1	HT	2.7	1.3	1.8
M2	WST	0.6	0.0	0.2
M2	FT	3.9	1.8	2.8
M2	HFT	3.3	2.8	3.0
M2	HT	2.7	2.6	2.0

TABLE S13

Sensitivity to Generation and Estimation Wavelet Mismatch: Simulated size and power estimates (%) for models P1-P5 and M1, M2 with nominal size of 5% and $N_1 = N_2 = 25$ realisations from each group. In all settings, the Haar wavelet is used for spectral estimation, but the following wavelets are used to generate the true spectra: Haar wavelets, Daubechies' least-asymmetric wavelets with 4 vanishing moments (V.M.) and Daubechies' extremal phase wavelets with 10 vanishing moments, respectively.

Model	Test	Haar wavelet (1 V.M.)	Daubechies' least-asymmetric (4 V.M.)	Daubechies' extremal phase (10 V.M.)
P6	WST	100.0	100.0	100.0
P6	FT	100.0	89.2	100.0
P6	HFT	100.0	89.5	87.6
P6	HT	100.0	68.7	66.3
P7	WST	100.0	100.0	100.0
P7	FT	100.0	92.0	93.0
P7	HFT	100.0	100.0	100.0
P7	HT	100.0	100.0	100.0
P8	WST	100.0	100.0	100.0
P8	FT	100.0	100.0	100.0
P8	HFT	100.0	100.0	100.0
P8	HT	100.0	100.0	100.0
P9	WST	100.0	100.0	100.0
P9	FT	100.0	100.0	100.0
P9	HFT	100.0	100.0	100.0
P9	HT	100.0	100.0	100.0
P10	WST	100.0	100.0	100.0
P10	FT	100.0	100.0	100.0
P10	HFT	92.0	92.5	92.0
P10	HT	100.0	100.0	100.0
P11	WST	100.0	100.0	100.0
P11	FT	100.0	100.0	100.0
P11	HFT	31.8	28.8	32.6
P11	HT	100.0	100.0	100.0
P12	WST	100.0	100.0	100.0
P12	FT	97.9	99.4	98.1
P12	HFT	9.1	7.1	7.9
P12	HT	98.3	98.8	99.1

TABLE S14

Sensitivity to the Change of Modelling Wavelet: Simulated power estimates (%) for models P6-P12 with nominal size of 5% and $N_1 = N_2 = 25$ realisations from each group. Different wavelets are used for the wavelet spectral estimation: Haar wavelets, Daubechies' least-asymmetric wavelets with 4 vanishing moments (V.M.) and Daubechies' extremal phase wavelets with 10 vanishing moments, respectively.

Name (Acronym)	Designed to ...	Strengths	Weaknesses
Wavelet Spectrum Test (WST)	Detect whether two groups display significant differences in the evolution of their spectral structures, and if so, the particular scales and times at which such differences occur.	Utilises CLT-type idea, therefore not sensitive to normality assumption when number of replicates is large.	Power heavily dependent on sample size.
Raw periodogram F-Test (FT)	Detect whether two groups display significant differences in the evolution of their spectral structures, and if so, the particular scales and times at which such differences occur.	Designed for (Gaussian) LSW processes, therefore can identify fine differences between spectra.	Sensitive to normality assumption.
Haar-Fisz Test (HFT)	Detect differences when the total power within a scale differs between groups.	Can identify differences when the total power within a scale differs between groups.	Reduced performance if there is similar overall power within each scale.
Haar Test (HT)	Detect whether groups evolve according to spectra that have the same shape (up to an additive constant) at each scale.	Can identify small differences between spectra.	It needs to be used in conjunction with WST or FT. The plot indicating where significant differences are located in the series is less easy to interpret than the 'barcode' plots of the other tests.

TABLE S15

A summary of the hypothesis tests developed in the manuscript.

- Bell-Pedersen, D., Cassone, V. M., Earnest, D. J., Golden, S. S., Hardin, P. E., Thomas, T. L., and Zoran, M. J. (2005). Circadian rhythms from multiple oscillators: lessons from diverse organisms. *Nature Reviews Genetics*, 6(7):544–556.
- Benjamini, Y. and Hochberg, Y. (1995). Controlling the false discovery rate: a practical and powerful approach to multiple testing *Journal of the royal statistical society. Series B (Methodological)*, *JSTOR*, 57:289–300.
- Bujdoso, N. and Davis, S. J. (2013). Mathematical modeling of an oscillating gene circuit to unravel the circadian clock network of *Arabidopsis thaliana*. *Frontiers in Plant Science*, 4:3.
- Cho, H. (2016). A test for second-order stationarity of time series based on unsystematic subsamples. *Stat*, 5(1): 262–277.
- Costa, M. J., Finkenstädt, B., Gould, P. D., Foreman, J., Halliday, K. J., Hall, A. J. W and Rand, D. A. (2011). Estimating periodicity of oscillatory time series through resampling techniques *University of Warwick. Centre for Research in Statistical Methodology*.
- Das, S. and Nason, G. P. (2016). Measuring the degree of non-stationarity of a time series. *Stat*, 5(1):295–305.
- Doyle, M. R., Davis, S. J., Bastow, R. M., McWatters, H. G., Kozma-Bognár, L., and Nagy, Ferenc and Millar, A. J. and Amasino, R. M. (2002). The ELF4 gene controls circadian rhythms and flowering time in *Arabidopsis thaliana*. *Nature*, 419(6902): 74–77.
- Dusik, V., Senthilan, P. R., Mentzel, B., Hartlieb, H., Wülbeck, C., Yoshii, T., Raabe, T. and Helfrich-Förster, C. (2014). The MAP kinase p38 is part of *Drosophila melanogaster*'s circadian clock. *PLoS genetics*, 10(8):e1004565.
- Edwards, K. D., Akman, O. E., Knox, K., Lumsden, P. J., Thomson, A. W., Brown, P. E., Pokhilko, A., Kozma-Bognar, L., Nagy, F., Rand, D. A., and Millar, A. (2010). Quantitative analysis of regulatory flexibility under changing environmental conditions. *Molecular systems biology*, 6(1): 424.
- Fan, J. and Lin, S.-K. (1998). Test of significance when data are curves *Journal of the American Statistical Association*, 93(443):1007–1021.
- Foley, J. A., DeFries, R., Asner, G. P., Barford, C., Bonan, G., Carpenter, S. R., Chapin, F. S., Coe, M. T., Daily, G. C., Gibbs, H. K. and others (2005). Global consequences of land use. *Science, American Association for the Advancement of Science*, 309(5734):570–574.
- Fryzlewicz, P. (2005). Modelling and forecasting financial log-returns as locally stationary wavelet processes. *Journal of Applied Statistics*, 32(5):503–528.
- Fryzlewicz, P. and Nason, G. P. (2006). Haar–fisz estimation of evolutionary wavelet spectra. *Journal of the Royal Statistical Society: Series B (Statistical Methodology)*, 68(4):611–634.
- Fryzlewicz, P. and Ombao, H. (2009). Consistent classification of nonstationary time series using stochastic wavelet representations. *Journal of the American Statistical Association*, 104:299–312.
- Fryzlewicz, P., Van Bellegem, S. and von Sachs, R. (2003). Forecasting non-stationary time series by wavelet process modelling. *Annals of the Institute of Statistical Mathematics*, 55(4):737–764.
- Goya, M. E., Romanowski, A., Caldart, C. S., Bénard, C. Y. and Golombek, D. A. (2016). Circadian rhythms identified in *Caenorhabditis elegans* by *in vivo* long-term monitoring of a bioluminescent reporter. *Proceedings of the National Academy of Sciences*, 201605769.
- Guo, W., Dai, M., Ombao, H. C. and von Sachs, R. (2003). Smoothing spline ANOVA for time-dependent spectral analysis. *Journal of American Statistical Association*, 98(463):643–652.
- Hanano, S., Domagalska, M. A., Nagy, F., and Davis, S. J. (2006). Multiple phytohormones influence distinct parameters of the plant circadian clock. *Genes to Cells*, 11(12):1381–1392.
- Harang, R. Bonnet, G. and Petzold, L. R. (2006). WAVOS: a MATLAB toolkit for wavelet analysis and visualization of oscillatory systems *BMC research notes, BioMed Central*, 5(1):163.
- Hargreaves, J. K., Knight, M. I., Pitchford, J. W., Oakenfull, R. and Davis, S. J. (2018). Clustering Nonstationary Circadian Rhythms using Locally Stationary Wavelet Representations. *SIAM Multiscale modeling and simulation*, 16(1):184–214.

- Hoagland, D. R. and Arnon, D. I. (1950). The water-culture method for growing plants without soil. *California Agricultural Experiment Station, Circular*, 347.
- Holan, S. H., Wikle, C. K., Sullivan-Beckers, L. E., and Cocroft, R. B. (2010). Modeling complex phenotypes: generalized linear models using spectrogram predictors of animal communication signals. *Biometrics*, 66(3):914–924.
- Killick, R., Eckley, I. A., and Jonathan, P. (2013). A wavelet-based approach for detecting changes in second order structure within nonstationary time series. *Electronic Journal of Statistics*, 7:1167–1183.
- Kon, N., Sugiyama, Y., Yoshitane, H., Kameshita, I. and Fukada, Y. (2015). Cell-based inhibitor screening identifies multiple protein kinases important for circadian clock oscillations. *Communicative & integrative biology*, 8(4):e982405.
- Krzemieniewska, K., Eckley, I. A., and Fearnhead, P. (2014). Classification of non-stationary time series. *Stat*, 3(1):144–157.
- Lagido, C., Pettitt, J., Flett, A. and Glover, L. A. (2008). Bridging the phenotypic gap: real-time assessment of mitochondrial function and metabolism of the nematode *Caenorhabditis elegans*. *BMC physiology*, 8(1):7.
- Leise, T. L., Indic, P., Paul, M. J. and Schwartz, W. J. (2013). Wavelet meets actogram. *Journal of biological rhythms*, SAGE Publications Sage CA: Los Angeles, CA, 28(1):62–68.
- Martinez J. G., Bohn K. M., Carroll R. J. and Morris J. S. (2013). A study of Mexican free-tailed bat chirp syllables: Bayesian functional mixed modeling for nonstationary acoustic time series. *Journal of American Statistical Association*, 108(502):514–526.
- McClung, C. R. (2006). Plant circadian rhythms. *The Plant Cell*, 18(4):792–803.
- McKay, J. L., Welch, T. D. J., Vidakovic, B. and Ting, L. H. (2012). Statistically significant contrasts between EMG waveforms revealed using wavelet-based functional ANOVA. *Journal of neurophysiology*, 109(2):591–602.
- Millar, A. J. and Carrington, J. T., Tee, W. V. and Hodge, S. K. (2015). Changing planetary rotation rescues the biological clock mutant lhy cca1 of *Arabidopsis thaliana*. *bioRxiv at Cold Spring Harbor Laboratory*.
- Minors, D. S. and Waterhouse, J. M. (2013). *Circadian rhythms and the human*. Butterworth-Heinemann
- Moore, A., Zielinski, T., and Millar, A. J. (2014). Online period estimation and determination of rhythmicity in circadian data, using the BioDare data infrastructure. *Methods in Molecular Biology*, 1158:13–44.
- Moore, D. S. (2007). The basic practice of statistics, (Vol. 2), *WH Freeman, New York*.
- Morris, J. S. (2015). Functional regression. *Annual Review of Statistics and Its Application*, 2:321–359.
- Morris J. S., Baladandayuthapani V., Herrick R. C., Sanna P. and Gutstein H. (2011). Automated analysis of quantitative image data using isomorphic functional mixed models, with application to proteomics data. *Annals of Applied Statistics*, 5(2A):894–923.
- Murashige, T. and Skoog, F. (1962). A revised medium for rapid growth and bio assays with tobacco tissue cultures *Physiologia plantarum*, 15(3):473–497.
- Nason, G. P. and Savchev, D. (2014). White noise testing using wavelets. *Stat*, 3(1):351–362.
- Nason, G. P., Von Sachs, R., and Kroisandt, G. (2000). Wavelet processes and adaptive estimation of the evolutionary wavelet spectrum. *Journal of the Royal Statistical Society: Series B (Statistical Methodology)*, 62(2):271–292.
- Nason, G. (2010). Wavelet methods in Statistics with R. *Springer Science & Business Media*.
- Nason, G. (2013). A test for second-order stationarity and approximate confidence intervals for localized autocovariances for locally stationary time series. *Journal of the Royal Statistical Society: Series B (Statistical Methodology)*, Wiley Online Library, 75(5):879–904.
- Nason, G. P. and Stevens, K. (2015). Bayesian Wavelet Shrinkage of the Haar-Fisz Transformed

- Wavelet Periodogram. *PLoS one, Public Library of Science*, 10(9):e0137662.
- Nicholson, F. A., Smith, S. R., Alloway, B. J., Carlton-Smith, C. and Chambers, B. J. (2003). An inventory of heavy metals inputs to agricultural soils in England and Wales. *Science of the total environment, Elsevier*, 311(1):205–219.
- Ogden, T. R. (1997). On preconditioning the data for the wavelet transform when the sample size is not a power of two. *Communications in Statistics-Simulation and Computation*, 26(2):467–486.
- Oh, H.-S., Ammann, C. M., Naveau, P., Nychka, D., and Otto-Bliesner, B. L. (2003). Multi-resolution time series analysis applied to solar irradiance and climate reconstructions. *Journal of atmospheric and solar-terrestrial physics*, 65(2):191–201.
- Perea-García, A., Andrés-Bordería, A., de Andrés, S. M., Sanz, A., Davis, A. M., Davis, S. J., Huijser, P., and Peñarrubia, L. (2015). Modulation of copper deficiency responses by diurnal and circadian rhythms in *Arabidopsis thaliana*. *Journal of experimental botany*, 67(1):391–403.
- Plautz, J. D., Straume, M., Stanewsky, R., Jamison, C. F., Brandes, C., Dowse, H. B., Hall, J. C. and Kay, S. A. (1997). Quantitative analysis of *Drosophila* period gene transcription in living animals. *Journal of Biological Rhythms, Sage Publications*, 12(3): 204–217.
- Price, T. S., Baggs, J. E., Curtis, A. M., FitzGerald, G. A. and Hogenesch, J. B. (2008). WAVECLOCK: wavelet analysis of circadian oscillation. *Bioinformatics, Oxford University Press*, 24(23): 2794–2795.
- Priestley, M. and Rao, T. S. (1969). A test for non-stationarity of time-series. *Journal of the Royal Statistical Society, Series B (Methodological)*, 31:140–149.
- Priestley, M. B. (1982). *Spectral analysis and time series*. Academic Press.
- Ramsay, J. O. and Silverman, B. W. (2005). *Functional Data Analysis*. Springer.
- Von Sachs, R. and Neumann, Mi. H. (2000). A Wavelet-Based Test for Stationarity. *Journal of Time Series Analysis, Wiley Online Library*, 21(5):597–613.
- Senesil, G. S., Baldassarre, G., Senesi, N. and Radina, B. (1998). Trace element inputs into soils by anthropogenic activities and implications for human health. *Chemosphere, Elsevier*, 39(2):343–377.
- Shumway, R. H. (1988). Applied Statistical Time Series Analysis. *Statistics & probability letters*, 63(3):307–314.
- Southern, M. M. and Millar, A. J. (2005). Circadian genetics in the model higher plant, *Arabidopsis thaliana*. *Methods in enzymology*, 393:23–35.
- Stiernagle, T. (1999). Maintenance of *C. elegans*. *C. elegans: A Practical Approach, Oxford University Press, Oxford, UK*, 2:51–67.
- Tavakoli, S. and Panaretos, V. M. (2016). Detecting and localizing differences in functional time series dynamics: a case study in molecular biophysics. *Journal of the American Statistical Association*, 111(515):1020–1035.
- Torrence, C. and Compo, G. P. (1998). A practical guide to wavelet analysis. *Bulletin of the American Meteorological Society*, 79(1):61–78.
- Van Bellegem, S. and von Sachs, R. (2008). Locally adaptive estimation of evolutionary wavelet spectra. *Annals of Statistics*, 36(4):1879–1924.
- Vidakovic, B. (2001). Wavelet-based functional data analysis: theory, applications and ramifications. *Proceedings of the 3rd Pacific Symposium on Flow Visualization and Image Processing*, Maui, HI.
- Vitaterna, M. H., Takahashi, J. S., and Turek, F. W. (2001). Overview of circadian rhythms. *Alcohol Research and Health*, 25(2):85–93.
- Zielinski, T., Moore, A. M., Troup, E., Halliday, K. J. and Millar, A. J. (2014). Strengths and limitations of period estimation methods for circadian data. *PLoS one, Public Library of Science*, 9(5):96462.

DEPARTMENT OF MATHEMATICS
UNIVERSITY OF YORK
YORK
YO10 5DD, UK
E-MAIL: marina.knight@york.ac.uk

DEPARTMENTS OF MATHEMATICS AND BIOLOGY
UNIVERSITY OF YORK
YORK
YO10 5DD, UK
E-MAIL: jon.pitchford@york.ac.uk

DEPARTMENT OF BIOLOGY
UNIVERSITY OF YORK
YORK
YO10 5DD, UK
E-MAIL: seth.davis@york.ac.uk